Ocean Engineering 293 (2024) 116619

Contents lists available at ScienceDirect

Ocean Engineering

journal homepage: www.elsevier.com/locate/oceaneng

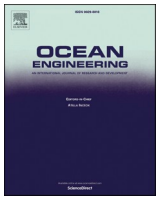

Research paper

Machine learning-based diagnosis in wave power plants for cost reduction using real measured experimental data: Mutriku Wave Power Plant

Fares M'zoughi [a,*], Jon Lekube [b], Aitor J. Garrido [a], Manuel De La Sen [c], Izaskun Garrido [a]

[a] Automatic Control Group—ACG, Institute of Research and Development of Processes—IIDP, Department of Automatic Control and Systems Engineering, Faculty of Engineering of Bilbao, University of the Basque Country—UPV/EHU, Po Rafael Moreno no3, 48013, Bilbao, Spain
[b] Biscay Marine Energy Platform—BiMEP, Atalaia 2 bajo, 48620, Armintza, Spain
[c] Automatic Control Group—ACG, Institute of Research and Development of Processes—IIDP, Department of Electricity and Electronics, Faculty of Science and Technology, University of the Basque Country—UPV/EHU, Bo Sarriena s/n, 48080, Leioa, Spain

ARTICLE INFO

Handling Editor: Prof. A.I. Incecik

Keywords:
Artificial Neural Network (ANN)
Annual Energy Production (AEP)
Capital Expenditure (CapEx)
Operational Expenditure (OpEx)
Oscillating water column (OWC)
Principal component analysis (PCA)
Linear discriminant analysis (LDA)
Support Vector Machine (SVM)
Wave energy

ABSTRACT

In comparison to wind farms, the relative scarcity of actual operational data from wave power plants has contributed to a significant research gap in the areas of wave farm forecasting and cost reduction. In this context, this manuscript presents a new Machine Learning-based Power Take-Off (PTO) diagnosis for wave energy generation farms which has the potential to serve as an extensive reference for other wave energy farms and offer substantial benefits to both investors and policymakers involved in the advancement of the emerging wave technologies. The suggested method has been employed at the Mutriku Wave Power Plant (WWP) to facilitate the implementation of predictive maintenance strategies and reduce the Levelized Cost of Energy (LCoE). Hence, the research study considers two main extraction methods, namely, Principal Component Analysis (PCA) and Linear Discriminant Analysis (LDA), used to select the most relevant features for OWC diagnosis. In addition, two classification methods have been considered: Support Vector Machine (SVM) and Multi-Layer Perceptron (MLP) Artificial Neural Network (ANN). The obtained data show that, although both methods allow to achieve an effective performance with an excellent degree of accuracy, the ANN-based method presents better results with 98% accuracy against 81% for the SVM when using PCA extraction method. Then, the developed classification-based OWC diagnosis has been used for the development of a predictive maintenance strategy at the Mutriku WPP, analyzing its impact on the economic indicators. The results indicate that, using the proposed predictive maintenance strategy, the OpEx may be decreased down to 17%, downtime may be decreased down to 55% and plant availability may be better up to 95%, leading to a 5% LCoE reduction.

1. Introduction

In pursuit of achieving climate neutrality by 2050, the European Union (EU) has heightened its climate objectives for the year 2030. To fulfill this commitment, the EU is placing a strong emphasis on expanding energy generation both at ocean and from the ocean. In the context of marine energy, the EU has outlined ambitious economic objectives for marine energy technologies in the European Strategic Energy Technology Plan (SET-Plan) in both wave and tidal energies (European Commission-SET Plan Secretariat, 2016). These objectives aim to decrease the LCoE in tidal stream generators to a minimum of 150 €/MWh by 2025 and 100 €/MWh by 2030, whereas in wave energy to a minimum of 200 €/MWh by 2025 and 150 €/MWh by 2030. Furthermore, additional climate goals have been established in the Offshore Renewable Energy Strategy, unveiled by the European Commission (EC) in November 2020 (European Commission, 2020a). The EU's goals for 2030 include the installation of 60 GW of offshore wind energy capacity and 1 GW of marine energy capacity encompassing wave and tidal energy. Looking ahead to 2050, the objectives become even more ambitious, with plans to install 300 GW of offshore wind energy and 40 GW of wave and tidal energies.

The EU's commitment to its goals has significantly propelled the advancement of tidal and wave technologies. Notably, the LCoE for tidal stream energy has been reduced by over 40% in the past three years alone, according to the EC's Joint Research Centre (Magagna and Tacconi, 2019). Tidal stream energy is currently approaching the threshold

* Corresponding author.
E-mail addresses: fares.mzoughi@ehu.eus (F. M'zoughi), jlekube@bimep.com (J. Lekube), aitor.garrido@ehu.eus (A.J. Garrido), manuel.delasen@ehu.eus (M. De La Sen), izaskun.garrido@ehu.eus (I. Garrido).

https://doi.org/10.1016/j.oceaneng.2023.116619
Received 4 August 2023; Received in revised form 17 November 2023; Accepted 18 December 2023
Available online 27 December 2023

of industrial deployment, exemplified by the EnFAIT project managed by Nova Innovation, which has deployed an array of three turbines. The array's capacity is set to be doubled, increasing from 300 kW to 600 kW, and it has already supplied power to the grid for over 24,000 h (ETIP Ocean, 2019; Nova). France achieved a significant milestone by connecting Sabella's D10 turbine, marking its first tidal turbine to be integrated into the national electricity network (Sabella). Orbital Marine Power's floating 2 MW turbine successfully accomplished one year of continuous operation within the FloTEC project, generating over 3.3 GW h of electric energy. This real-world conditions test validated the technology, the investigated Operational and Maintenance (O&M) costs, and the demonstrated value to the potential market (IEA-OES, 2018). Improvement of blade survivability and performance tests are being carried out using Magallanes Renovables' tidal turbine in emulated harsh conditions within the NEMMO project, which aims to improve performance and reliability (European Commission, 2019a). In addition, revolutionary PTO designs are being tested at sea on a full-scale and small-scale basis as part of the TiPA project (European Commission, 2017) and PowerKite project (European Commission, 2019b). The TiPA project is testing a direct drive turbine that does not require a gearbox (TiPA). While a 500 kW device was deployed off the coast of North Wales as part of the PowerKite project. On the other side, Wave Energy Converter (WEC) designers are presently focusing on enhancing the performance of their systems via design changes. Consequently, it will permit the technique to be demonstrated at a higher Technology Readiness Level (TRL) and then commercialized (Magagna, 2020). The WaveBoost project created and tested a novel Power Take-Off technology that increased the reliability and performance of CorPower Ocean's point-absorber buoy (European Commission, 2020b). Further Power Take-Off design innovations maybe seen in the EMERGE project and IMAGINE project (Wave Energy Scotland) (European Commission, 2018) with the re-adaptation of aerospace technology for new PTOs. The EMERGE project has created an original ballscrew-based PTO which reached TRL7. The Electromechanical Generator PTO of Umbra has been integrated in a real-sea scale testing of the EEL Energy tidal device (Umbra Cuscinette, 2017). The wave power plant of Mutriku has validated and de-risked innovative wave energy developments and improved TRL. First, OceanTEC tested its Wells turbine, as part of the pre-commercial public procurement launched by EVE that enabled the installation of Marmok-A-5 in open-sea operating conditions at BiMEP since December 2016 and sharing the resulting data (European Commission, 2019c). And in 2017 the OPERA project tested the biradial impulse turbine of Kymaner in one of the chambers (Magagna, 2019). Later in 2018, the Wells turbine in Marmok-A-5 has been replaced by the tested biradial turbine. Wedge Global is coordinating the SEA-TITAN project, which has been engaged in the design, construction, experimentation, and validation of an innovative second-generation Direct Drive PTO. This advanced system aims to optimize energy production while safeguarding equipment in challenging environmental circumstances. (European Commission SEA-TITAN, 2019). The TRL of Wave technology is currently considered at 7. Only onshore devices, such as the multiple OWC Mutriku WPP in the Basque Country, have shown consistent power generation and can be classified as TRL 8 (Magagna, 2019).

Enhancing availability, capacity factor, and Annual Energy Production (AEP) is another way for reducing LCoE. This can be accomplished by implementing effective monitoring and maintenance strategies to ensure optimal system performance. Maintenance plays a critical role in minimizing downtime throughout the plant's lifespan, ultimately resulting in improved availability, power production, capacity factor, and AEP. Therefore, decreasing O&M expenses is an efficient way for decreasing the Levelized Cost of Energy (Ren et al., 2021).

A power plant's daily operations require an effective and reliable maintenance strategy. The maintenance staff should visit the plant regularly to help avoid failures. Needless regular maintenance visits, on the one hand, are sometimes unproductive and expensive due to the considerable need for maintenance technician and equipment. A reduced maintenance visit frequency, on the other hand, may cause higher failure rate and, as a consequence, longer downtime. Therefore, scheduling the adequate maintenance frequency and implementing the best maintenance strategy have a significant impact on the plant's productivity. The implementation of an optimal maintenance system can lead to 11%–18% reduction in O&M costs (Zhu et al., 2019).

Maintenance approaches are typically classified into reactive, proactive, and opportunistic categories, depending on when maintenance activities are conducted. The reactive maintenance, also known as corrective maintenance, involves performing maintenance only after a failure has occurred. This approach is suitable for situations where downtime-related maintenances are minimal, enabling high availability. Thus, the reactive strategy is effective when used in relatively little farms with high reliability (Karyotakis and Bucknall, 2010). Conversely, the proactive maintenance focuses on scheduled inspections and replacements before failures happen. By addressing small faults before they escalate into major failures, this approach aims to prevent disruptions. Various maintenance methods maybe classified as proactive strategy, including preventive, condition-based, and predictive maintenance (Jiang, 2011). The opportunistic approach involves the integration of planned preventive and corrective actions with unplanned preventive tasks aimed at addressing potential issues with deteriorating components in the future. This strategy encompasses a mix of planned and unplanned actions to optimize maintenance operations (Thomas et al., 2008).

In both onshore and offshore power plants, a proactive maintenance strategy is highly recommended, which involves gathering time-based and sensor-based data to design and employ an appropriate maintenance plan (Yeter et al., 2020; Tomás-Rodríguez and Santos, 2019). However, dealing with the vast quantity of information collected and the multitude of variables measured can pose challenges in data processing. To address this, feature extraction techniques are employed to reduce redundant information and the dimensionality of the data across various fields (Sklansky, 1978; Boonyakitanont et al., 2020; Peng et al., 2002). One commonly used feature extraction algorithm is Principal Component Analysis (PCA), a multivariate statistical method designed to reduce the dimensionality of a problem for effective data analysis (Abdi and Williams, 2010). PCA examines data from multiple observations described by dependent and inter-correlated variables. The goal is to extract vital information from the data and transform it into a collection of distinct orthogonal variables referred to as principal components (Hasan and Abdulazeez, 2021). Other renowned feature extraction technique is the Linear Discriminant Analysis (LDA) (Izenman, 2013). LDA aims to find a projection hyperplane that minimizes the variance between different classes and maximizes the distance between the projected means of the classes. The objectives of both methods can be achieved by solving the eigenvalue problem, where the corresponding eigenvectors define the relevant hyperplane (Wen et al., 2018).

In order to use the extracted data to monitor the health of the plant and identify possible failures, recognizing failure patterns in the data is sought. Therefore, many works studied the development of classification models (Kiang, 2003; Liu et al., 2006; Verma and Tiwary, 2014). These would include the nonparametric *k*th-Nearest Neighbor method which employs "feature similarity" to estimate the values of new data points that will be assigned a value based on how close it matches the points in the training set (Wong and Lane, 1983). The logistic models, which describe data and explain the correlation between one dependent binary variable and nominal independent variables (Cox, 2018). The decision tree (C4.5) that makes use of a splitting technique that recursively divides a set of instances into scattered subsets (Quinlan, 2014). Also, the Multivariate Discriminant Analysis which creates a discriminant function by maximizing the ratio of "between groups" variance and "within groups" variance (Fisher, 1936).

Support Vector Machine (SVM) is a well-established machine

learning technique specifically designed to addressing classification problems with large datasets (Suthaharan and Suthaharan, 2016). Its applicability is particularly prominent in multi-domain scenarios within a big data environment. However, it's important to note that SVM involves complex mathematical computations and can be computationally demanding (Pisner and Schnyer, 2020). Nonetheless, SVM demonstrates strong generalization capability, allowing it to achieve high accuracy in classifying machine conditions and diagnosing faults (Widodo and Yang, 2007; Lee, 2021). However, Artificial Neural Networks (ANN) proved to be a potential classification method when it comes to big data classification and pattern recognition problems (Holyoak, 1987; Sierra-García and Santos, 2021). It has the ability of performing non-linear analysis in complex forecasting applications (Kumar et al., 2011; Yang et al., 2022). A comparative study between SVM and ANN has been performed in (Ahmad et al., 2014) and results showed that both classification methods are competitive in terms of performance and accuracy. Therefore, the choice is made based on the nature of application, type of data and desired objectives.

In this work, a classification-based diagnosis method for cost reduction in wave power plant farms using experimental data has been proposed to deal with maintenance problems in a in order to reduce the economic costs of energy production. The suggested approach is tested on the case of Mutriku WPP where the Oscillating Water Columns of the plant suffer from unwanted vibrations. These vibrations if left untreated will lead to undesired failures and breakages. The research work first employs two feature extraction techniques, namely PCA and LDA to select the relevant data to be used for the classifiers. Then two classification methods are studied namely the SVM and ANN classification techniques to compare their accuracy. Based on the proposed diagnosis strategy, the economic costs of the energy production are computed to study the impact of the strategy in costs reduction in wave energy power plants. It is important to note that, as of July 2023, there has been a notable lack of research dedicated to wave power plant prognosis and cost reduction. Consequently, this real-world case study has the potential to serve as an extensive reference for other wave energy farms, offering substantial benefits to both investors and policymakers involved in the advancement of these emerging renewable technologies.

The rest of the paper has been organized as follows: Section 2 presents the problem of the selected study case as the PTO vibration in OWCs in the WPP of Mutriku, Spain. Section 3 presents the methods used for data processing and feature extraction using PCA and LDA. Section 4 presents the Machine Learning-based oscillating water column diagnosis developed to predict the health status of the OWC units based on two classification methods SVM and ANN. Section 5 explains the economic assumptions and indicators used to evaluate the operation of the considered plant. Section 6 introduces the obtained results of the trained classification models performance and accuracy and the economic improvement of AEP, OpEx and LCoE reduction. Finally, Section 7 finishes the article with some concluding remarks.

2. Problem statement

In July 2011, the Mutriku wave power plant, located in the Bizkaia, Spain, was officially commissioned by the Basque Energy Agency (Ente Vasco de la Energía - EVE). The establishment of this facility was made possible through the support of the 6th Framework Program of the EC (specifically, the Nereida MOWC project) and the Basque Government (Torre-Enciso et al., 2009). The plant itself is situated onshore and is integrated into the harbor's breakwater, as depicted in Fig. 1. As of 2019, the Mutriku WPP became part of the Basque marine energy test center BiMEP (Biscay Marine Energy Platform). By July 2022, the WPP completed 11 years of operation during which it supplied over 2.7 GW h of energy to the grid.

The plant consists of 16 OWC to generate electricity from wave energy. All 16 OWC units are equipped with a Wells turbine coupled to an electric generator of 18.5 kW rated power bring up the total installed capacity to 296 kW. All capture chambers are identical in shape and size with 4.5m in length, 3.1m width and 9.7m height above MLWS (Mean Low Water Springs) level as shown in Fig. 2. The PTO system consists of two co-rotating monoplane Wells turbines coupled to induction generator with squirrel-cage rotor of 18.5 kW. The generator uses a voltage of 460V and has a rated speed of 3000 rpm.

Over the past decade of its operation, the Mutriku WPP has encountered various instances of degradation and component failures. The details of these events are provided in the subsequent subsection.

2.1. Operating in harsh environment

The harsh conditions at the coast of Mutriku, due to the exposure to a saline environment and elevated levels of humidity, contribute to the fatigue of several components, which affects the performance of the OWC and leads to failure of the power system. In fact, the continuous contact with saline corrodes many parts along with strong oscillatory forces that OWCs are exposed to will subsequently lead to deterioration or breakage (Lekube et al., 2018a). Moreover, the air turbine used in the PTOs is of the Wells turbine type. This type of turbine is known to exhibit a stalling behavior once a strong wave enters the capture chamber producing a high airflow speed but the generator cannot increase its speed swiftly hence slowing the turbine (Fs et al., 2017; M'zoughi et al., 2020a). Hence, during the stalling phenomenon, the blades are subject to high airflow speed, which increases the vibration.

Table 1 illustrates some examples of failures and breakage in OWC system (Lekube et al., 2018a).

2.2. OWC vibration issues

All the aforementioned damages, which might arise in any OWC system they consequently, lead to increase in the vibration.

The turbine T03 was reported to suffer from bearing problem. The bearing problem is related to lack of lubrication, which lead to friction-induced overheat that causes expansion of the bearing ring. Also, exposure to the low and high temperature during winter and summer

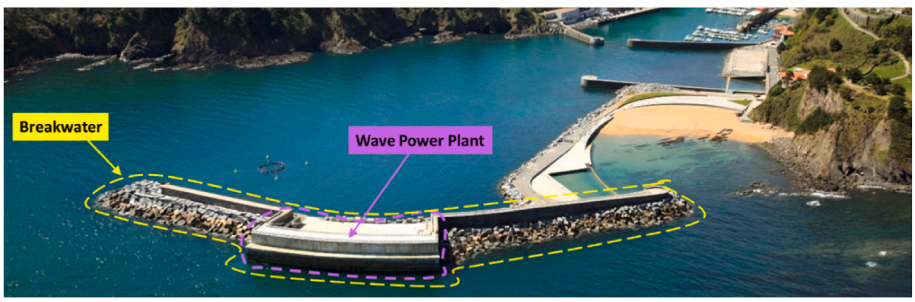

Fig. 1. The breakwater and the Mutriku wave power plant from above.

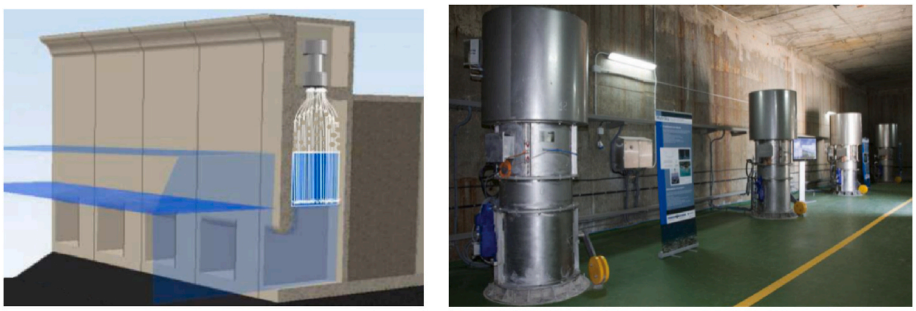

Fig. 2. The Multiple Oscillating Water Columns of Mutriku Wave Power Plant. (a) Front view of the Capture chambers. (b) Power Take- Off room above the capture chambers.

Table 1
Types of failure and problems occurred on OWCs in Mutriku WPP.

Component	Cause	Damages
Wells turbine	Exposure to saltwater and material fatigue from strong airflows	
Generator	Exposure to saltwater and/or strike by broken blades	
Bearing cover	Excessive axial force induced in the turbine shaft leads to bearings rubbing against the inside of the generator cover	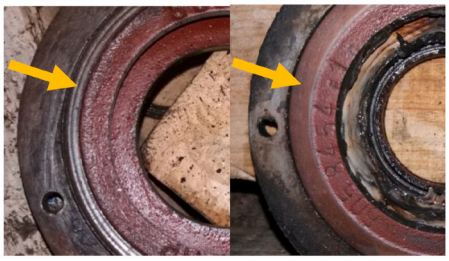
Cooling system	Salt accumulation	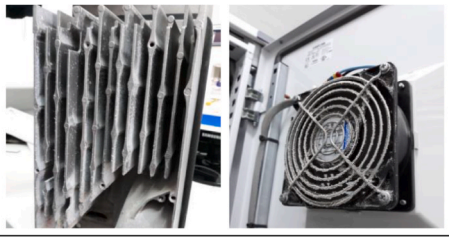

changes the lubricant viscosity leading to extra strain on the bearing balls when the lubricant is cold and thick or leading to friction when the lubricant leaks out because it is hot and thin. Another recurrent cause of bearing problems is contamination, which occurs after particles enter the bearing raceway and get pressed between it and the balls. As they keep rolling over the particles, craters are created leading to excessive heat generation and vibration.

The turbine T06 was reported to suffer from resonance problem. The resonance issue occurs when the oscillating force imposed on the PTO system reaches one of its natural frequencies causing an excess in vibration. An example of this behavior can be seen in the PTO's vibration velocity versus the rotational speed illustrated in Fig. 3.

The turbine T07 was reported to suffer from unbalance problem. Unbalance issue is related to loss of symmetry due to unequal distribution of mass caused by salt accumulation on some blades of the Wells turbine or corrosion. This unbalance lead the mass axis to differ from the bearing axis. The uneven mass, combined with the radial acceleration produced by rotation, produces a centrifugal force during rotation. This imposes force on the bearings and/or bearing vibration.

Figs. 4–6 show the collected data of vibration in turbines T03, T06 and T07 recorded for 24 h on 15/09/2021 in Mutriku WPP.

As depicted in the preceding figures, the vibrations observed can surpass 20 mm/s. If these unwanted vibrations are not addressed, they have the potential to adversely impact the performance of the OWC system and potentially contribute to degradation and component breakage. In Figs. 5 and 6, there is a noticeable abrupt cessation of vibrations between the 2.5 and 3.3 time intervals. This cessation is a result of a system shutdown, initiated to prevent further vibrations and potential damage. These planned shutdowns of the system can sometimes extend for several hours, resulting in production losses.

2.3. OWC maintenance

Preventive maintenance is performed on a regular basis at Mutriku WPP to prevent failures or breakages. Regular maintenance is carried out on a monthly or annual basis, based on the amount of wear on each part, including mechanical, electrical and control equipment, and server checking. A visual inspection of the plant is done during scheduled monthly maintenance. Several components are subject to revision, including sensors, emergency stop switches, fasteners, the generator terminal box, cables and its trays, fresh water piping, sprinklers, and damper actuators. Furthermore, a comprehensive inspection is conducted to detect any indications of corrosion. Additionally, the cooling fan in the power converter room undergoes thorough examination. (Lekube et al., 2018a).

At present, the operation and maintenance responsibilities for the plant lie with BiMEP. Fortunately, accessibility is not a concern for the Mutriku WPP. However, for remote or offshore installations, maintenance operations become crucial. The occurrence of frequent unpredictable failures can lead to production losses resulting from unavailability. As a result, strategically planned predictive and preventive maintenance measures are highly valued in such cases.

3. Methodology

In order to investigate and propose an efficient approach for the preventive maintenance of OWCs, it is crucial to analyze the data gathered from Mutriku, as illustrated in Fig. 7.

Examining and analyzing the recorded vibration velocity across various months and weather conditions can aid in the identification and diagnosis of potential problems and faults within the OWC system. Fig. 7 illustrates the block diagram representing the adopted methodology for diagnosing the specific type of failure in the OWC unit. This diagnostic process facilitates the scheduling of future maintenance activities, thereby minimizing operational expenses.

3.1. Data collection

As a research facility of BiMEP, the Mutriku WPP has implemented a range of sensors to enable the gathering of crucial data. These sensors capture various parameters, including pressure in the capture chamber, pressure drop, generated power, voltage, current, and more (refer to Fig. 8).

Data acquisition from the sensors and conversion of analog and fieldbus signals are facilitated by the Beckhoff system. To connect the Beckhoff system with the Programmable Logic Controller (PLC), the Control Techniques' CTNet network is utilized. This CTNet fieldbus operates as a Token Ring network with a capacity of 5 Mbit, enabling peer-to-peer communication. Communication between the SCADA system and the PLC system occurs through an Object Linking and Embedding (OLE) for Process Control (OPC) server/client configuration (Lekube et al., 2018b).

3.2. Data pre-processing

The collected data include information about the time and date of operation, operation mode, damper position which, in the case of the Mutriku OWC, is the valve plate angular position (in degrees), the generator rotational speed (in rpm), the pressure (in Pa), the PTO vibration (in mm/s), the generated power (in kW), the voltage (in V) and current (in A) as shown in Fig. 9. It's to be noted that collected data vary from one wave farm to another depending on the type of WEC and its location. This may include external environmental measurements related to wind and waves which may be very helpful to implement prognosis and diagnosis strategies for cost reduction. However, in the study case of Mutriku WPP, the WEC are fixed OWCs hence the wind conditions would have no effects on the structure's stability. As for the wave conditions, the wave elevation within the fixed capture chamber is transformed to oscillating airflow and pressure hence the pressure data is sufficient to establish the relationship.

To prevent biases in the data, such as missing or out-of-range values, inaccurate data readings with aberrant values are first deleted. In addition, Inter-Quartile Range (IQR) is used to remove data outliers (Vinutha et al., 2018). In order to prevent false positives caused by particular wave circumstances and to guarantee the persistence of

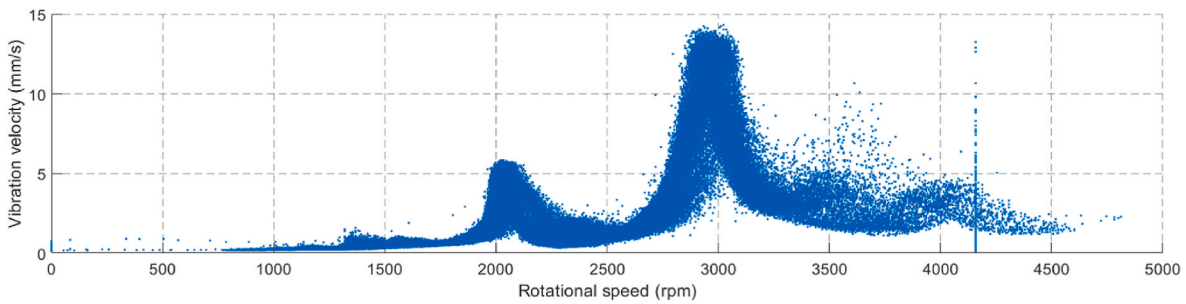

Fig. 3. A 24 h measured vibration velocity vs. rotational speed of turbine T06 in Mutriku WPP on 15/09/2021 with resonance problem.

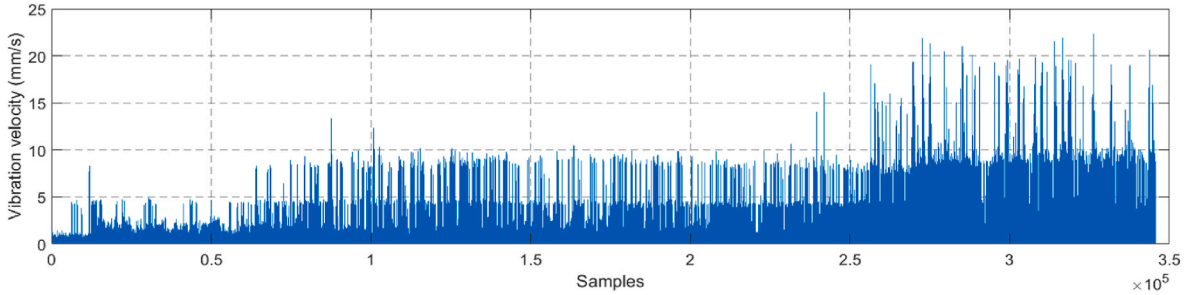

Fig. 4. A 24 h measured vibration velocity of turbine T03 with bearing problem in Mutriku WPP on 15/09/2021.

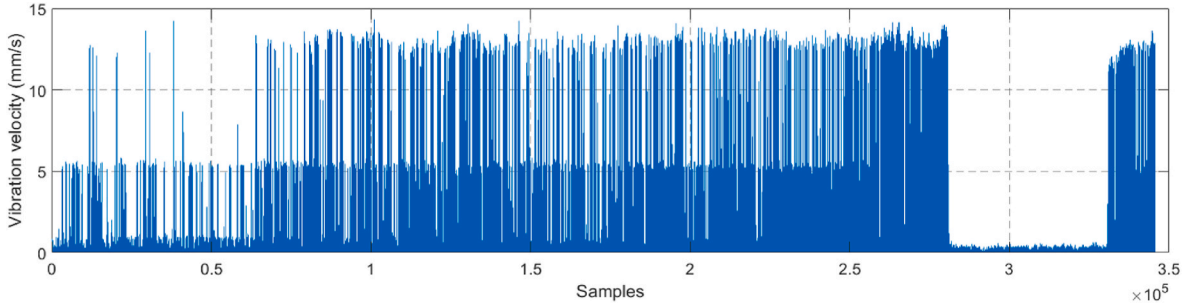

Fig. 5. A 24 h measured vibration velocity of turbine T06 with resonance problem in Mutriku WPP on 15/09/2021.

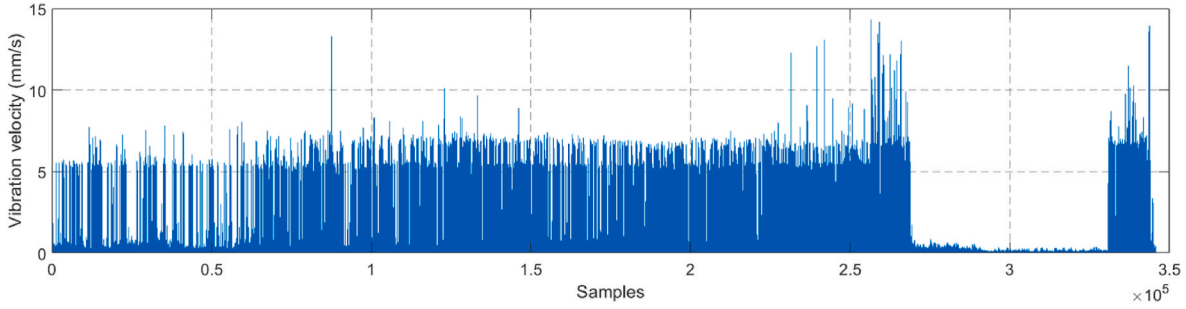

Fig. 6. A 24 h measured vibration velocity of turbine T07 with unbalance problem in Mutriku WPP on 15/09/2021.

anomalous occurrences throughout the course of 5-min intervals, the original 10 Hz sampled signals are then down sampled into 5-min averages. Lastly, data binning is used to minimize the effects of small observation errors (Davis et al., 2007).

3.3. Feature extraction

Feature extraction is a pre-processing technique that helps simplify the computation process and reduce the complexity of a dataset. Dealing with a large number of features can lead to substantial computational and memory burdens during classifier training and classification. In high-dimensional data, identifying patterns can be challenging. Hence, Principal Components Analysis (PCA) and Linear Discriminant Analysis (LDA) are widely employed methods for data analysis, as they aid in uncovering meaningful patterns and reducing the dimensionality.

3.3.1. Principal Components Analysis

PCA is a technique used to detect patterns within a dataset and represent the data in a way that emphasizes their similarities and differences. It is a mathematical method known as an orthogonal linear transformation, where the data is transformed to a new coordinate system. In this new coordinate system, the first coordinate captures the maximum variance among all possible projections of the data (Vidal et al., 2016).

To ensure that the mean of the data is zero, the matrix of data $\boldsymbol{X}$ with dimensions $(n\ x\ m)$ consisting of n_o observations of n_v variables needs to be centered. This involves calculating the mean vector, which is defined as:

$$\mu_i = \frac{1}{n_o}\sum_{i=1}^{n_v} X_i \tag{1}$$

here the X_i are column vectors of the matrix of data $\boldsymbol{X}$.

To center the data matrix, the mean vectors are subtracted from all column vectors, resulting in:

$$\boldsymbol{X} = \left[(X_1 - \mu_1), \cdots (X_i - \mu_i), \cdots \left(X_{n_v} - \mu_{n_v}\right)\right] \tag{2}$$

The correlation between features is determined by the covariance of data matrix $\boldsymbol{X}$ as:

$$\boldsymbol{\Sigma} = \frac{1}{n_v}\sum_{i=1}^{n_v}(X_i - \mu_i)(X_i - \mu_i)^T = \frac{1}{n_v}\boldsymbol{X}\boldsymbol{X}^T \tag{3}$$

The eigenvalues and eigenvectors are computed by solving the equation $\boldsymbol{X}\,\boldsymbol{X}^T$ as (Izenman, 2013; Vinutha et al., 2018):

$$\boldsymbol{\Sigma} = V\Lambda V^{-1} = V\Lambda V^T \tag{4}$$

in this equation, $\boldsymbol{V}$ represents a unitary matrix consisting of the

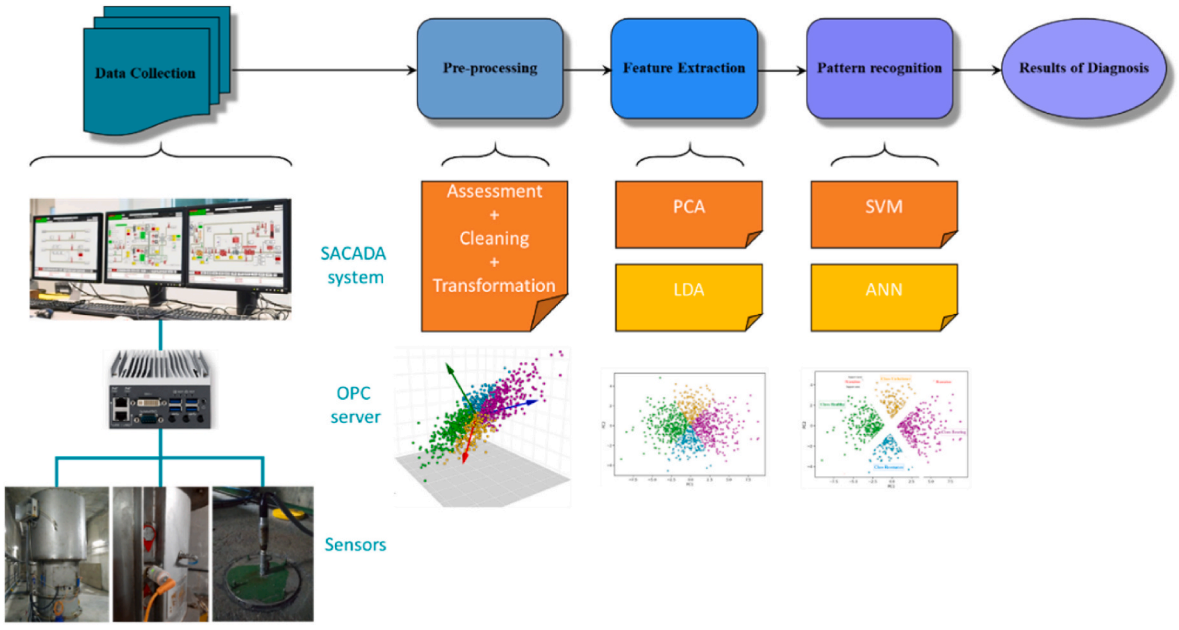

Fig. 7. Block diagram of the data-based OWC diagnosis for Mutriku wave power plant.

eigenvectors $\boldsymbol{v_i}$, while $\boldsymbol{\Lambda}$ represents a diagonal matrix that contains the corresponding eigenvalues λ_i.

To organize the principal components (PCs) in a meaningful way, the eigenvalues λ_i are used to sort them in descending order, resulting in the rearranged matrix $\boldsymbol{\Lambda_a}$. Simultaneously, the eigenvectors are reordered accordingly, leading to the matrix $\boldsymbol{V_a}$ (Vidal et al., 2016). The cumulative energy content for each eigenvector can then be computed from $\boldsymbol{\Lambda_a}$ using the following expression:

$$g_i = \sum_{k=1}^{i} \Lambda_{a_{kk}} \quad (i = 1, \ldots, n_v) \tag{5}$$

To determine the number of PCs to be selected, a threshold value θ is defined. The selected number of principal components, denoted as S, is determined by ensuring that the cumulative energy content of these components satisfies the following condition (Abdi and Williams, 2010; Izenman, 2013):

$$g_S / g_{n_v} \geq \theta \tag{6}$$

A feature vector $\boldsymbol{U}$ is constructed by selecting the S eigenvectors from the matrix $\boldsymbol{V_a}$ that correspond to the highest eigenvalues λ_i.

Finally, the original data set $\boldsymbol{X}$ is transformed from its original axes to the axes represented by the PCs by means of the feature vector $\boldsymbol{U}$. This transformation is accomplished by multiplying the transpose of the vector $\boldsymbol{U}$ by the original data set $\boldsymbol{X}$, resulting in:

$$P = U^T X \tag{7}$$

The PCA algorithm is summarized and explained by the pseudo-code of Algorithm 1.

Algorithm 1. PCA

Algorithm 1: PCA	
1	Load data $\boldsymbol{X}$
2	Calculate the mean vectors μ_i using (1).
3	Center the data matrix $\boldsymbol{X}$ using (2).
4	Compute the covariance, eigenvalues and eigenvectors using (3) and (4).
5	Reorder eigenvaleus matrix $\boldsymbol{\Lambda_a}$ in descending λ_i order and eigenvectors matrix $\boldsymbol{V_a}$.
6	Retain $\boldsymbol{S}$ first major PCs using (5) and (6) to from $\boldsymbol{U}$ with the biggest eigenvectors λ_i.
7	Reconstruct the feature data $\boldsymbol{P}$ by projection using (7).

3.3.2. Linear Discriminant Analysis

The most often used classical linear technique to reduce

Fig. 8. Mutriku's OWC sensors. (a) Chamber pressure sensor. (b) PTO vibration sensor.

T03_20210715_S1.csv

	A	B	C	D	E	F	G	H
	T032021071551							
	Date	Time	T03_AUTOMATIC	T03_DamperActualPosition_Deg	T03_Motor_rpm	T03_Power_k...	T03_Pressure_Pa	T03_Vibration_mmps
	Datetime	Text	Number	Number	Number	Number	Number	Number
1	Date	Time	T03_AUTOMATIC	T03_DamperActualPosition_Deg	T03_Motor_rpm	T03_Power_kW	T03_Pressure_Pa	T03_Vibration_mmps
2	14/07/2021	23:00:00,000	10	89	1008	-0.18	634.5	0.395
3	14/07/2021	23:00:00,250	10	89	1002	-0.18	244.5	0.375
4	14/07/2021	23:00:00,500	10	89	1002	-0.18	0.5	0.375
5	14/07/2021	23:00:00,750	10	89	990	-0.18	-292.5	0.375
6	14/07/2021	23:00:01,000	10	89	996	-0.18	-487.5	0.365
7	14/07/2021	23:00:01,250	10	89	1014	-0.18	-780.5	0.365
8	14/07/2021	23:00:01,500	10	89	1026	-0.18	-634.5	0.365
9	14/07/2021	23:00:01,750	10	89	1038	-0.21	-682.5	0.365
10	14/07/2021	23:00:02,000	10	89	1044	-0.21	-780.5	0.365
11	14/07/2021	23:00:02,250	10	89	1068	-0.21	-683.5	0.365
12	14/07/2021	23:00:02,500	10	89	1068	-0.18	-488.5	0.365
13	14/07/2021	23:00:02,750	10	89	1080	-0.21	-439.5	0.365
14	14/07/2021	23:00:03,000	10	89	1086	-0.21	-439.5	0.385

Fig. 9. Collected data of an OWC for turbine T03 on 15/07/2021.

dimensionality is LDA. Within the feature-based projection space, LDA looks for a transformation matrix W that will optimally increase the ratio of the between-class disperse and decrease the within-class disperse matrix.

LDA search for a transformation matrix W, which will maximize the ratio of the between-class disperse and will minimize the within-class disperse matrix within the feature-based projection space (Yu and Yang, 2001). LDA is an approach to obtain the linear sets of characteristics that best distinguishes between multiple classes of events or objects.

The matrix of within-class distribution S_W may be described by (Yu and Yang, 2001; Ghassabeh et al., 2015):

$$S_w = \sum_{i=1}^{c} \sum_{x \in Ci} (x - m_i)(x - m_i)^t \tag{8}$$

where c represents the number of classes while C_i represents the set of data in the ith class, and m_i represents the mean of the ith class. It's to be noted that the matrix of within-class distribution is a representation of the level of scattering inside classes as the sum of the covariance matrices of every class.

Another relevant parameter is the between-class scatter matrix, which maybe defined as (Yu and Yang, 2001; Ghassabeh et al., 2015):

$$S_B = \sum_{i=1}^{c} n_i (m_i - m)(m_i - m)^t \tag{9}$$

A criterion function is then defined using S_W matrix of the within-class scatter and S_B matrix of the between-class scatter to obtain the transformation matrix W described by (Yu and Yang, 2001; Ghassabeh et al., 2015):

$$J(W) = \frac{|\widetilde{S}_B|}{|\widetilde{S}_W|} = \frac{|W^t S_B W|}{|W^t S_W W|} \tag{10}$$

The transformation matrix W is the one will maximize the criterion function $J(W)$. The generalized eigenvectors w_i in the columns of the optimum transformation matrix W correspond to the biggest eigenvalues in:

$$S_B W_i = \lambda_i S_W W_i \tag{11}$$

LDA seeks to identify a combination of features by effectively differentiating between various object classes. If S_W is full-rank, W may be calculated via the eigenvectors of $S_W^{-1} S_B$.

Both LDA and PCA utilize linear transformations to enhance the variance in a reduced dimension. Nonetheless, unlike PCA, LDA focuses on identifying linear discriminants that optimize the variance among different categories while minimizing the variance within each class.

The LDA algorithm is summarized and explained by the pseudo-code of Algorithm 2.

Algorithm 2. LDA

Algorithm 2: LDA	
1	Load data $\boldsymbol{X}$.
2	Classify the data to $\boldsymbol{c}$ classes.
3	Calculate the matrix of within-class distribution S_W using (8).
4	Calculate the matrix of within-class distribution S_B using (9).
5	Compute the criterion $J(W)$ using (10).
6	Find the transformation W matrix by maximizing $J(W)$ using (11).

3.3.3. OWC feature extraction for the vibration problem

The pre-processed datasets are employed to extract features that depict the health status of the plants. Conducting a PCA on the OWC data from the Mutriku WPP allows us to identify the most significant features for our study. The scree plot presented in Fig. 10 illustrates the cumulative variance explained by each additional principal component derived from PCA or each discriminant component obtained from LDA. Additionally, the blue bars indicate the variance explained by every component in percent.

According to the scree plot depicted in Fig. 10(a), the first principal

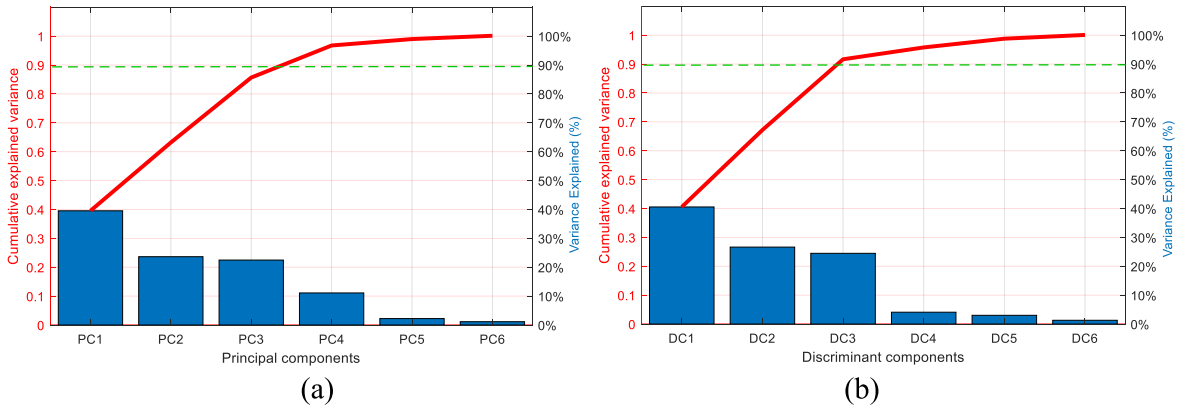

Fig. 10. Scree plot of cumulative explained variance versus the components. (a) Explained variance obtained from PCA. (b) Explained variance obtained from LDA.

component accounts for 39.53% of the variance, whereas the second, third, and fourth components explain 23.64%, 22.48%, and 11.09%, respectively. Therefore, a total of 4 components is needed to achieve a cumulative explained variance of 96.74%. Conversely, based on the scree plot in Fig. 10(b), the first discriminant component explains 40.88% of the variance, whereas the second and third components explain 26.43% and 24.78%. In this case, 3 components are required to reach a cumulative explained variance of 92.09%.

According to the LDA the focus should be around the first three components, namely the vibration velocity, the rotational speed and the pressure features, whereas according to the PCA the focus should be around the first four components which correspond to the vibration velocity, rotational speed, pressure and generated power features. Since the generated power is and output variable of the OWC and doesn't contribute to the variation, only the vibration velocity, the rotational speed and the pressure features will be used to design the classifier.

Fig. 11 displays scatter plots of the first two features obtained from data collected at the Mutriku wave power plant on 15/09/2021. The scatter plots include measurements from a healthy Wells turbine, as well as three turbines exhibiting various defects, namely unbalanced, bearing, and resonance problems.

The relationship between the average vibration and the rotational speed of the rotor can be observed from the data shown in Fig. 11. It is evident that for each turbine, there are two distinct peaks recorded around 1900 rpm and 2900 rpm. In the case of a healthy turbine, the vibration typically reaches a maximum of 3 mm/s. However, in the case of unhealthy turbines, the vibration levels can exceed 6 mm/s around 2800 rpm for unbalance problems, 8 mm/s around 2838 rpm for bearing problems, and 11 mm/s around 2940 rpm for resonance problems.

Figs. 12–14 present a scatter plot of the first three features based on data collected from the Wells turbine T03 with bearing problem, turbine T06 with resonance problem and turbine T07 with unbalance problem at the Mutriku WPP on 15/09/2021. The 3D scatter plot clearly demonstrates that the variation in vibration is influenced not only by the rotational speed but also by the pressure.

From the 3D plots of Figs. 12–14 it is clear that the three turbine issues (i.e. bearing, resonance and unbalance) have a distinct pattern. In fact, in the case of bearing problem two predominant peaks a small one around 1940 and a bigger around 2850. Whereas in the case of bearing problem two predominant peaks a small one around 2060 and a bigger around 2940. Finally, in the case of unbalance problem two predominant peaks a small one around 1925 and a bigger around 2815.

Based on the above results, it has been decided to use the first three components contributing to the vibration of the OWC system to design the classifier.

4. Classification-based OWC diagnosis

A classifier will be developed and trained using the processed data to classify the various health statuses of the OWC based on the input

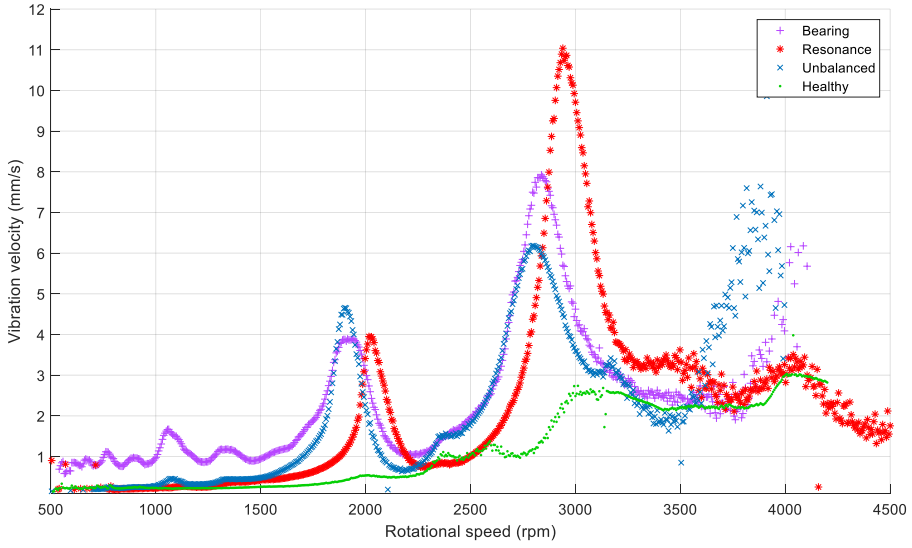

Fig. 11. 2 features scatter plot of the mean vibration vs. the angular velocity in four turbines in OWCs on 15/09/2021 at Mutriku WPP.

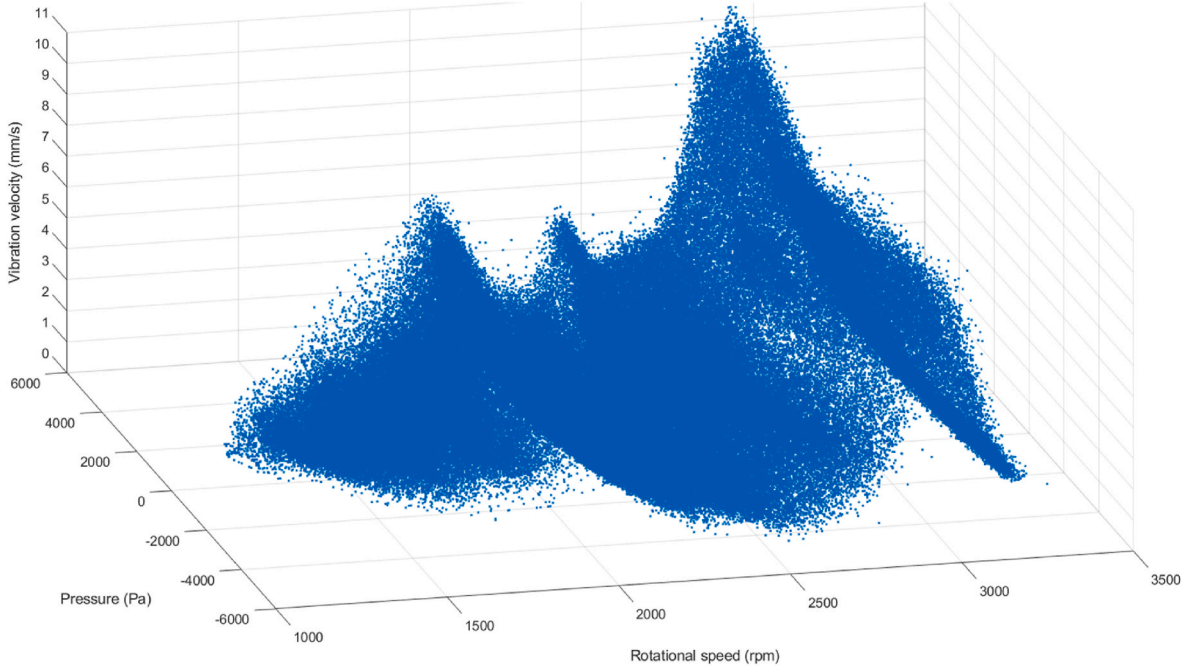

Fig. 12. Scatter plot of the relationship between vibration, angular velocity, and pressure in turbine T03 with bearing issues on 15/09/2021 at the Mutriku WPP.

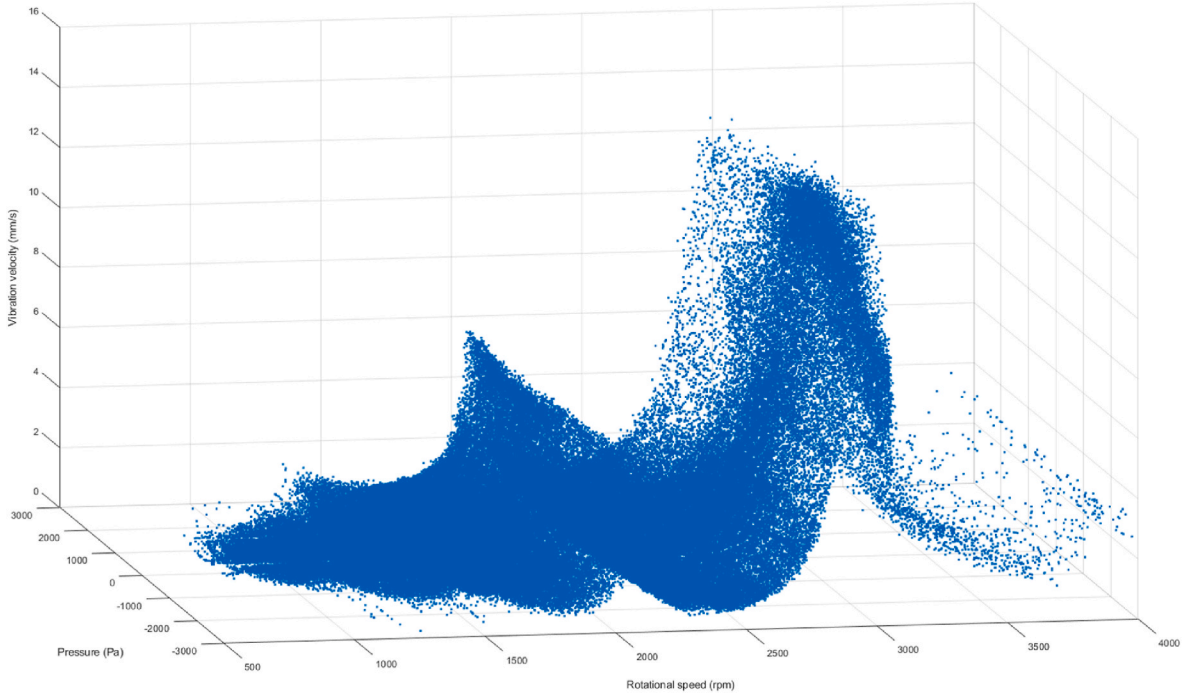

Fig. 13. Scatter plot of the relationship between vibration, angular velocity, and pressure in turbine T06 with resonance problem on 15/09/2021 at the Mutriku WPP.

features. In this work, two classification methods have been considered the SVM and ANN.

The objective of the suggested Machine Learning-based PTO diagnosis is to enhance the efficiency of the maintenance scheduling by using predictive maintenance strategy instead of preventive maintenance strategy.

4.1. Multi-Layer Perceptron

Multi-layer Perceptron (MLP) feedforward networks, which are often employed in pattern recognition and classification tasks, are the ANN structure selected for this problem (Zhang et al., 1998). The developed MLP consists of multiple neurons in the input layer representing the features of the plant data such as vibration velocity, rotational speed, pressure, etc. and a single neuron in the output layer for the stat of the monitored OWC and multiple hidden layer as shown in Fig. 15. While

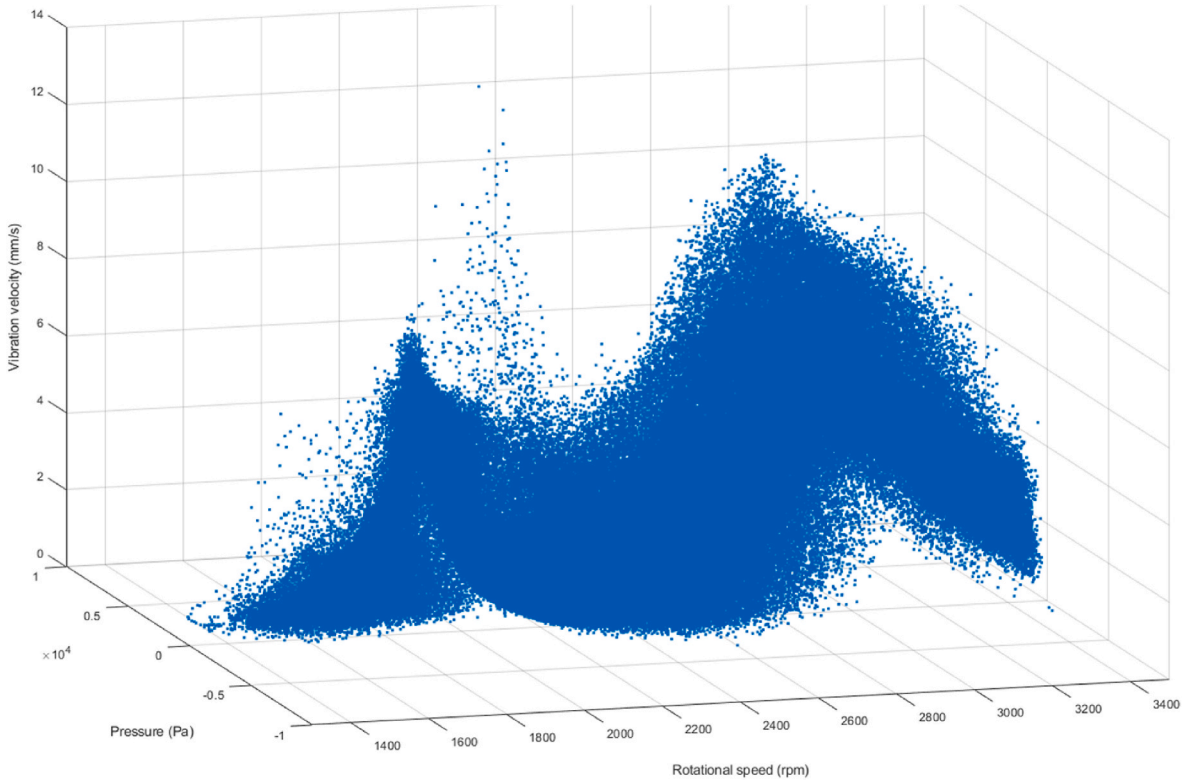

Fig. 14. Scatter plot of the relationship between vibration, angular velocity, and pressure in turbine T07 with unbalance problem on 15/09/2021 at the Mutriku WPP.

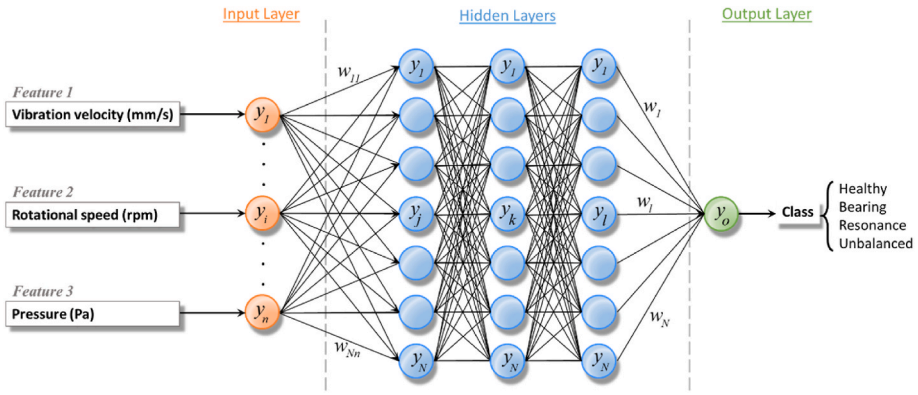

Fig. 15. Proposed MLP structure for the PTO fault recognition.

the neurons utilized in the output layer have linear activation function, those employed in the hidden layers have hyperbolic tangent activation functions.

The Levenberg-Marquardt Algorithm (LMA), which features both the gradient descent and Gauss-Newton approaches, was used to train the designed ANN (Hagan and Menhaj, 1994).

The weights linking the neurons can be updated by the LMA to enhance the result. The following update expression may be used to accomplish this:

$$w_{ji}(p+1) = w_{ji}(p) + \Delta w_{ji}(p) \tag{12}$$

Where $w_{ji}(p+1)$ represents the updated weight, $w_{ji}(p)$ represents the present weight and $\Delta w_{ji}(p)$ represents the weight's correction attained by the selected training algorithm.

LMA has been employed as the learning approach for the network's training (Hagan and Menhaj, 1994; M'zoughi et al., 2020b). LMA was created to minimize functions that are summation of squares of nonlinear functions and uses Newton's approach (Wilamowski and Yu, 2010). The algorithm's goal is to reduce the performance index by updating the ANN weights by (Suratgar et al., 2005):

$$\Delta W = \left[\nabla^2 F(W) + \mu I\right]^{-1} \nabla F(W) \tag{13}$$

here W represents the weights vector. $F(.)$, $\nabla F(.)$, $\nabla^2 F(.)$ represent performance index, gradient and Hessian matrix, respectively, while μ and I represent the learning rate and identity matrix.

The performance index can be explained as follows:

$$F(W) = \sum_{j=1}^{N} E_j^2(W) = E^T(W)\ \ E(W) \tag{14}$$

where $E(.)$ represents the error between the network's and the desired outputs.

The gradient of the performance index may be determined by:

$$\nabla F(W) = 2J^T(W)\,E(W) \tag{15}$$

where *J(W)* represents the Jacobian matrix defined as (Ampazis and Perantonis, 2000):

$$J(W) = \begin{pmatrix} \frac{\partial E_1(W)}{\partial W_1} & \frac{\partial E_1(W)}{\partial W_2} & \cdots & \frac{\partial E_1(W)}{\partial W_n} \\ \frac{\partial E_2(W)}{\partial W_1} & \frac{\partial E_2(W)}{\partial W_2} & \cdots & \frac{\partial E_2(W)}{\partial W_n} \\ \vdots & \vdots & \ddots & \vdots \\ \frac{\partial E_N(W)}{\partial W_1} & \frac{\partial E_N(W)}{\partial W_2} & \cdots & \frac{\partial E_N(W)}{\partial W_n} \end{pmatrix} \tag{16}$$

where n represents the total of training patterns.

The Hessian matrix may therefore be explained as:

$$\nabla^2 F(W) = 2J^T(W).J(W) + 2\sum_{j=1}^{N} E_j(W).\nabla^2 E_j(W) \tag{17}$$

In this work, the Mean Squared Error (MSE) has been used as performance indicator of the trained network. MSE is one of the metrics frequently utilized in prediction applications (M'zoughi et al., 2020b; M'zoughi et al., 2020c) and is defined as:

$$MSE = \frac{1}{n}\sum_{i=1}^{n}(Y_i - \widehat{Y}_i)^2 \tag{18}$$

here Y_i is the target output being the class and $\widehat{Y}_i$ is the ANN-predicted output by the.

The Levenberg-Marquardt Algorithm is summarized by the pseudo-code of Algorithm 3.

Algorithm 3. LMA

Algorithm 3: LMA

```
Randomly initialize weights w_ji(p) and biases b_ji.
Obtain the predicted output Ŷ.
Calculate the error and MSE using (18).
While (stopping criterion is not met) do
    Calculate the performance index Δw_ji(p) using (13)-(17).
    Update the network weights w_ji(p+1) using (12).
    Recalculate the error and MSE(i) using (18).
    If ( MSE(i+1) < MSE(i) ) then
        μ = 0.1 μ
    else
        Discard the new weights w_ji(p+1).
        μ = 10 μ
    end if
End while
```

Obtained results of training the MLP model are illustrated in Fig. 16. The performance is high with the best validation performance at a low MSE of 3.16 10-8 obtained at 34 epochs.

4.2. Support Vector Machine

A SVM is a discriminative classifier described by a separating hyperplane. SVM has been extensively developed and used in pattern recognition and classification problems (Suthaharan and Suthaharan, 2016; Pisner and Schnyer, 2020). SVM is a collection of associated supervised learning techniques. In essence, SVM is a hyperplane classifier. Finding a hyperplane that has the biggest margin of separation between the positive training instances and the negative training instances is required for training an SVM classifier (Awad et al., 2015). SVM's ability to deal with nonlinearly separable data is one of the primary causes for its widespread use. Given training samples are shown as pairs (x_i, y_i), here x_i represents the vector of weighted features of the training sample and $y_i \in \{1, -1\}$ represents the label of the sample. For data that can be separated linearly, we may identify a hyperplane $f(x) = 0$, which splits them as:

$$f(x) = \sum_{i=1}^{n} w_i x_i + b = 0 \tag{19}$$

here w represents a n-dimensional vector and b represents a scalar. Both w and b define the location of the separating hyperplane.

For each i either:

$$\begin{cases} w.x_i - b > 1 & \text{for } x_i \text{ of the first class.} \\ w.x_i - b \le 1 & \text{for } x_i \text{ of the second class.} \end{cases} \tag{20}$$

The hyperplane that offers the largest margin is called the separating hyperplane. The ideal hyperplane may be achieved by solving problem (21), taking into account the noise with slack variables ξ_i and error penalty E_p:

$$\min_{w,b,\xi} P(w,b,\xi) = \frac{1}{2}\langle w.w\rangle + \frac{E_p}{2}\sum_{i=1}^{n}\xi_i^2 \tag{21}$$

here ξ_i is the distance between the margin and example x_i lying on the wrong side of the margin.

The complexity of the computations can be reduced by transforming the problem involving Kuhn-Tucker conditions into an equivalent Lagrange dual problem.

$$V(\alpha) = \sum_{i=1}^{l}\alpha_i - \frac{1}{2}\sum_{i,j=1}^{l}\alpha_i\alpha_j y_i y_j K(x_i.x_j) \tag{22}$$

subject to

$$\sum_{i=1}^{l} y_i\alpha_i = 0, C \ge \alpha \ge 0, i = 1,2,\ldots,l \tag{23}$$

The function $K(x_i.x_j)$ is known as the kernel function, which returns a dot product of the original data points' feature space mappings. The dual problem consists of the same number of variables as the training data.

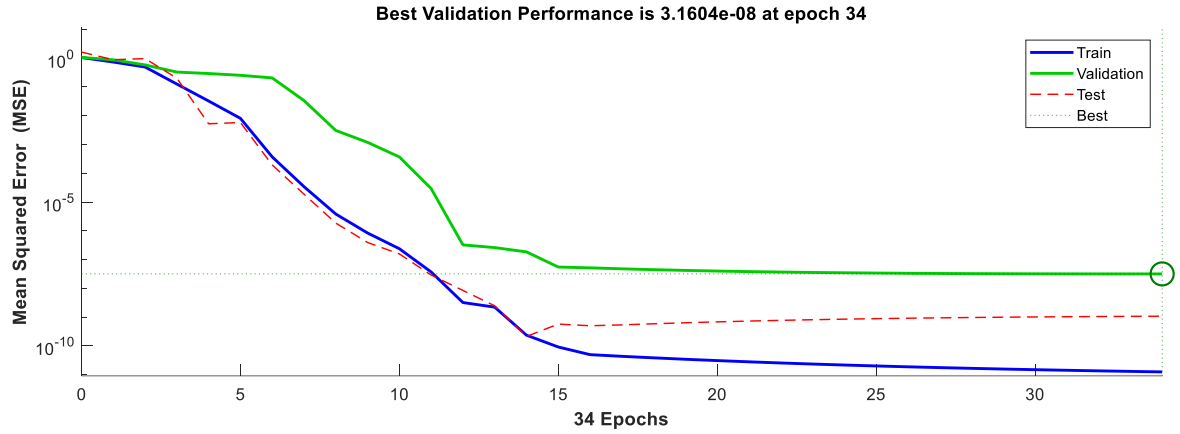

Fig. 16. Training performance of the ANN Model.

The Karush-Kuhn-Tucker theorem states that the associated should not be 0, in order for the training input-output pair (x_i. y_i), to satisfy the equality criterion (Ghosh et al., 2019). In this case, the training instance x_i is a Support Vector (SV). The number of SVs is considerably lower than the number of training samples making SVM computationally very efficient. SVM is extremely computationally effective since the number of SVs is much smaller than the number of training instances. For the classification problem, SVM is an efficient classifier.

The SVM algorithm is summarized by the pseudo-code of Algorithm 4.

Algorithm 4. SVM

Algorithm 4: SVM	
1	Load extracted features dataset $\boldsymbol{X}$ as pairs (x_i, y_i).
2	Classify the data to classes.
3	Identify hyperplanes between classes using (19) and (20).
4	Calculate the kernel function $K(x_i.x_j)$.
5	Choose the ideal hyperplane by minimizing problem (21) using (22) and (23).
6	**If** Accuracy and Validity are not met **then**
7	Return to step 3.
8	**else**
9	Return the best hyperplane as the Separating Hyperplane.
10	**End if**
11	End

Obtained results of training the SVM model are illustrated in Fig. 17. The performance is high with the best validation performance at a MSE of 3.9757 10-6 obtained at 56 epochs.

4.3. Classification-based OWC health diagnosis

The developed MLP consists of three neurons in the input layer representing the vibration speed, the rotational speed and the pressure and a single neuron in the output layer for the state of the monitored OWC and multiple hidden layer as shown in Fig. 15.

The accuracy of the predicted output is proven by the perfect regression curves (R = 1) shown in Fig. 18(a) and very low errors from the Error Histogram of Fig. 18(b).

Fig. 19(a) demonstrates a minimal level of confusion between classes, as the accuracy of correct predictions is 98% and the rate of incorrect predictions is only 2%. The Receiver Operating Characteristic (ROC) in Fig. 19(b) illustrates the outstanding performance of the ANN classifier, with an Area Under Curve (AUC) of 0.98.

Same as the ANN classifier model, the SVM model has been trained with the 3 main features extracted and with 4 classes. The training of the SVM using the OWC processed data has provided the results of Fig. 20.

In Fig. 20(a), it can be observed that the level of confusion between classes is low. The accuracy of correct predictions between classes is 89%, while the rate of incorrect predictions is 11%. The ROC plot depicted in Fig. 20(b) demonstrates that the SVM classifier exhibits a commendable performance, with an AUC of 0.98.

5. Techno-economic assessment

The techno-economic assessment of a wave energy plant may be achieved by calculating the economic indicators. This may be achieved by using two computational models namely the Operational and Maintenance (O&M) model and the Cost model as shown in Fig. 21. Both models use Input data from the wave energy conversion plant.

The O&M model outputs are utilized to minimize the reliance on assumptions regarding the inputs for the Cost model. The Annual Energy Production (AEP) and OpEx values, computed using the O&M model, are incorporated into the cost model to calculate metrics such as LCoE and other economic indicators.

5.1. Economic assumptions

Some presumptions are established in the early phases of the concept creation in order to do an economic assessment. The project's preliminary CAPEX and OPEX figures can be obtained by reverse calculations. The following parameters require specific values to be assumed in order to complete the reverse computation:

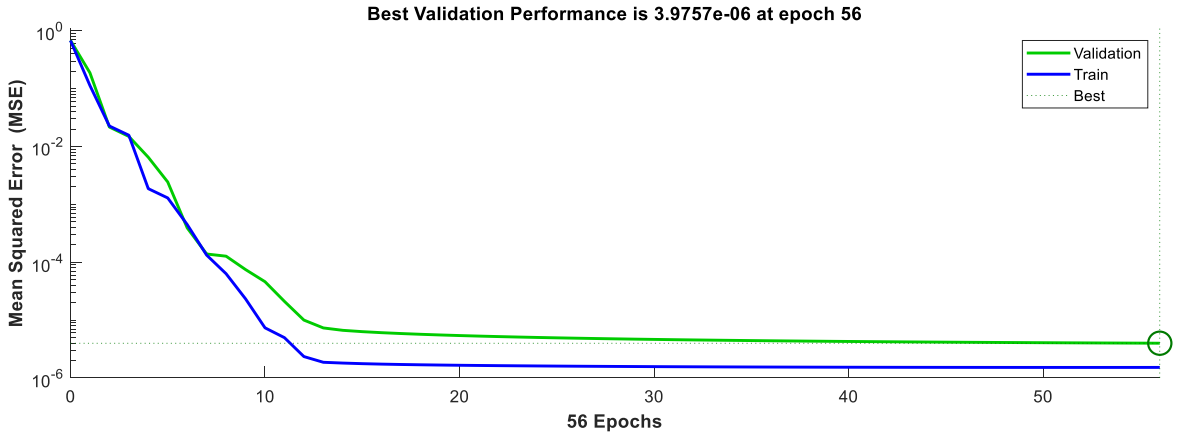

Fig. 17. Training performance of the SVM Model.

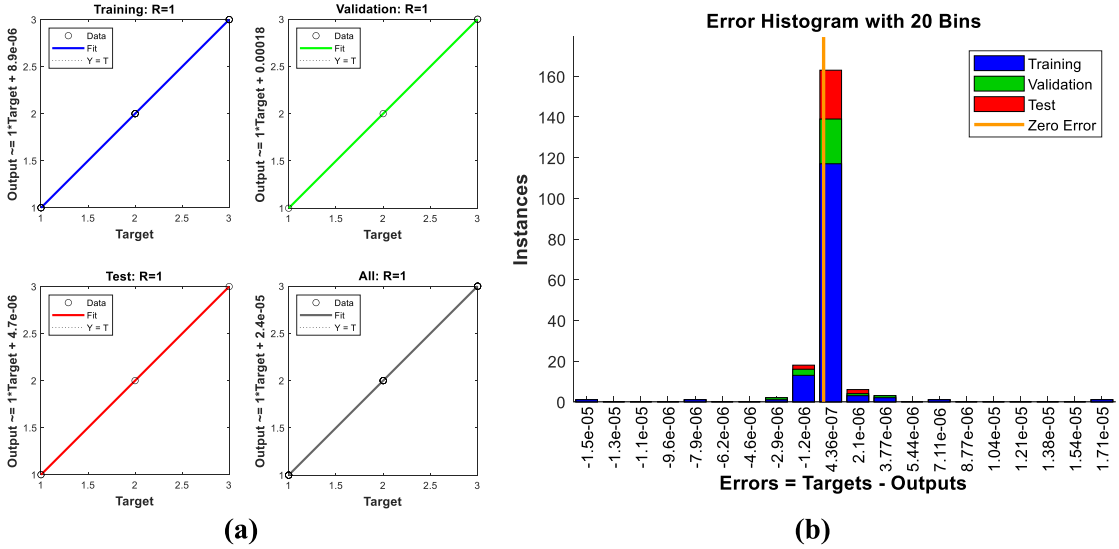

Fig. 18. Accuracy of the ANN classifier. (a) Regression curves plot. (b) Error Histogram plot.

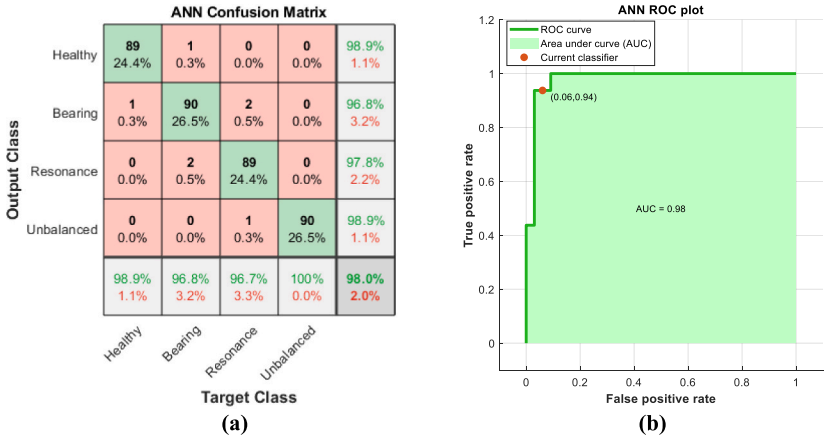

Fig. 19. Classification performance of the ANN classifier. (a) Confusion plot. (b) ROC plot.

Discount rate, or ***r***, is often considered to remain constant during the course of the project. The discounted cash flow analysis uses the discount rate to determine the present value of future cash flows. It is the rate of return that investors could expect from an investment of equivalent risk. Hence, it depends on the investor's risk perception and willingness to invest. While the discount rate *r* for mature technologies (e.g. carbon, wind …) is about 5–10%, for new technologies (e.g. wave, tidal …) it is approximately 12–18% (Pecher and Kofoed, 2017).

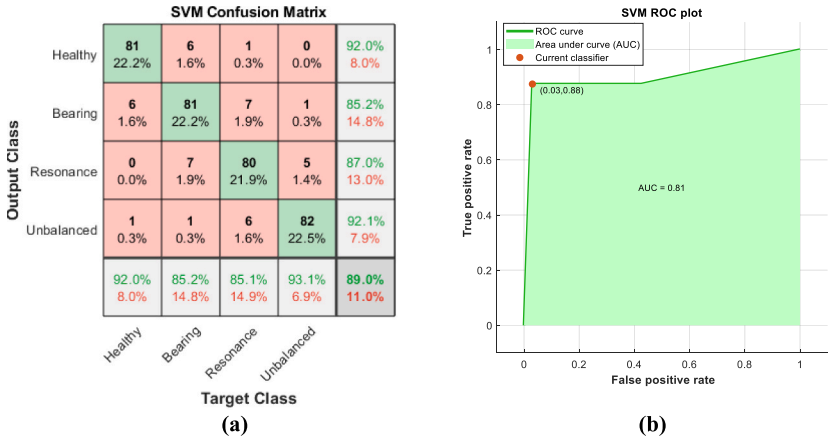

Fig. 20. Classification performance of the SVM classifier. (a) Confusion plot. (b) ROC plot.

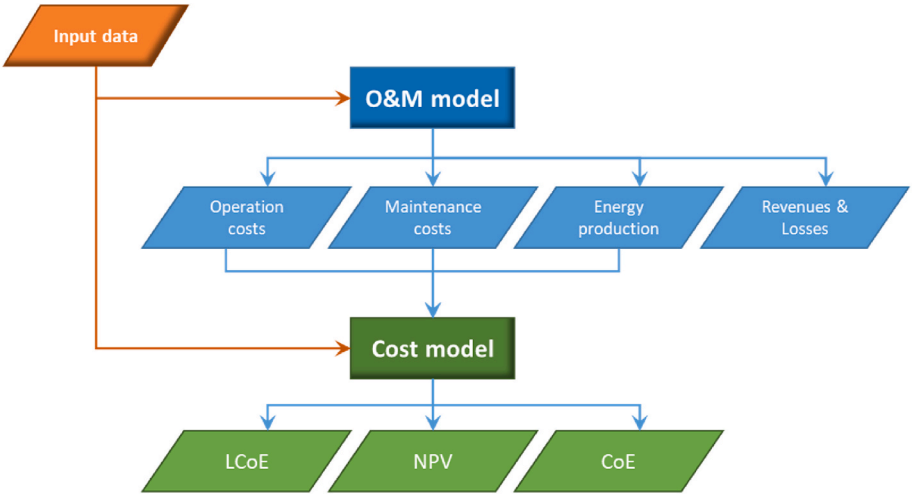

Fig. 21. Relationship between the input data, O&M costs and energy costs.

Therefore, a 15% discount rate is assumed appropriate for the multiple oscillating water column plant of Mutriku since tidal technologies are more mature.

Project lifetime, or ***n***, is the estimated life span of an established project. 20–25 years are typical lifespans associated to maritime renewable energy projects (Paredes et al., 2019; Têtu and Fernandez Chozas, 2021). A lifetime of the wave power plant project in Mutriku has been set to $n = 20$.

Availability factor, or ***a*%**, represents the total time of a producing power plant (uptime) by the total time of a producing plant and total time of non-producing plant (downtime) as:

$$a\% = \frac{uptime}{uptime + downtime} \times 100 \tag{24}$$

5.2. Economic indicators

The capacity factor (C_f) is a key metric for describing the mean load of any power facility (Izquierdo et al., 2010; Ibarra-Berastegi et al., 2018). C_f may be described as the output energy of the plant over the maximum energy capacity. Hence, the annual C_f may be calculated as the power output during a year over the maximum power capacity by a year as:

$$C_f = \frac{Annual\ \ Average\ \ Power}{Rated\ \ Power\ \ Capacity} = \frac{Annual\ \ Energy\ \ Production\ \ (AEP)}{24 \times 365 \times TOWC \times P_{Rated}} \tag{25}$$

where P_{Rated} is the rated power of one OWC unit (in kW) and $TOWC$ is the total number of operating OWC in the farm.

C_f can be calculated on a monthly or seasonal basis but since it is low during the summer and high during the winter, an annual value would be more appropriate.

The present value (PV) is the value of an expected income stream determined over the lifetime of the project. The present value of a future cash flow X can be calculated as:

$$PV(X) = \sum_{t=0}^{n} \frac{X_t}{(1+r)^n} \tag{26}$$

The Levelized Cost of Energy (LCoE) is an economic indicator of the total cost of constructing and operating a power plant over its lifetime divided by the total power produced during that lifetime (Bruck et al., 2018). LCoE is a useful metric that allows the comparison of the competitiveness between different projects, energy sources and different technologies:

$$LCoE = \frac{PV(CapEx + OpEx)}{PV(AEP)} = \frac{\sum_{t=0}^{n} \frac{(CapEx_t + OpEx_t)}{(1+r)^n}}{\sum_{t=0}^{n} \frac{AEP_t}{(1+r)^n}} \tag{27}$$

5.2.1. CapEx breakdown

For a wave energy project, all of the expenses connected with project development, deployment, and commissioning up to the start of the

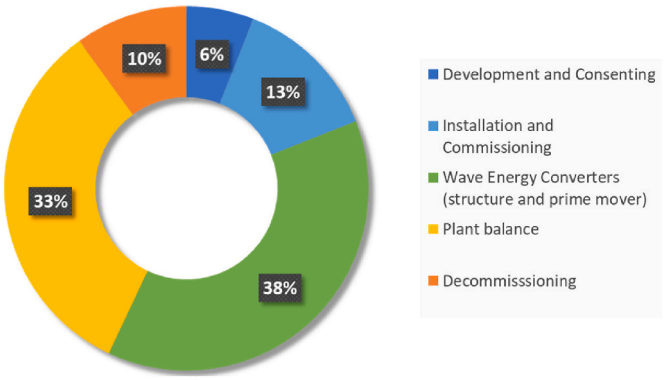

Fig. 22. CAPEX breakdown of costs for different WEC cost centers.

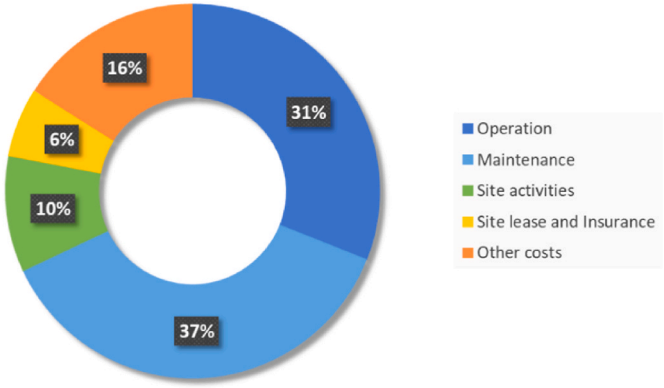

Fig. 23. OpEx breakdown of costs for different cost centers.

wave farm's operation may be summed up as Capital Expenditure (CapEx). Decommissioning is also a part of CapEx after a project is finished. A. Têtu et *al.* provide comprehensive assessment of the literature on CapEx expenses in (Têtu and Fernandez Chozas, 2020).Costs found in this class consist of expenses associated to the different stages of developing a WEC farm from inception all the way to the handing over of the WEC farm to the client as detailed in Fig. 22.

5.2.2. OpEx breakdown

A wave energy project's Operational Expenditures (OpEx) include all costs related to running the farm once a takeover certificate is given. These costs include those for all O&M tasks and those related to the site leasing and insurance. Fig. 23 summarizes the OpEx's expenses detailed breakdown gathered in the comprehensive assessment of the literature provided in (Têtu and Fernandez Chozas, 2020).

The yearly OpEx may be calculated as a proportion of the CapEx for a WEC farm where there is little available data. According to the literature, estimates of total annual OpEx typically fall between 1.5% and 9% of CapEx (Magagna, 2019; Pecher and Kofoed, 2017; Têtu and Fernandez Chozas, 2021). This is because of several reasons (e.g., single prototype or utility-scale project, distance from the shore, floating or submerged technology, advanced or traditional O&M strategies applied, etc.).

For instance, the OPERA project (OPERA Project, 2019) shown that, depending on the deployment site and the dimension of the farm, the OpEx might get as low as 1.8%–2.2% of the CapEx when adequate novel O&M approaches are used. The knowledge gained from the offshore wind energy business, where yearly OpEx amounts to 4.5% of CapEx (Pecher and Kofoed, 2017) and 3% of CapEx (IRENA, 2017), respectively, might be applied to utility-scale projects. Following a 2018 international survey of wave energy developers, the following figures were discovered: annual OpEx for a utility scale project is in the interval [4%–5%] of CapEx, for a small WEC array OpEx is 6% of CapEx and for a single WEC device is in the interval [6%–9%] of CapEx.

6. Results and discussion

6.1. Classification performance and diagnosis

A comparative study between the SVM and ANN classifiers has been performed to evaluate the accuracy against the number of features used. Both classifiers have been compared while paired with PCA or LDA feature extraction algorithms. The results of the simulation are illustrated in Figs. 24 and 25.

The ANN classifier offers higher accuracy than that of the SVM classifier this may be due to the number and type of the feature inputs of this problem. In addition, with both classifiers the PCA outperformed the LDA algorithm. This may be due to the complex correlation between data and the difficulty of separation between the classes.

The accuracy of the trained ANN and SVM classifiers using both feature extraction methods PCA and LDA is summarized in the following table. Table 2 shows the accuracy of the SVM and ANN obtained when using PCA which found 4 main features and when using LDA which found 3 main features.

6.2. Economic evaluation

All the Wells turbines at the Mutriku wave plant have exactly the same design. However, turbines T01 and T16 do not accumulate enough pressure at the inlet because chambers are not completely sealed and need a structural redesign. Therefore, these two turbines did not generate any electricity during the analyzed period and only 14 OWCs were operational.

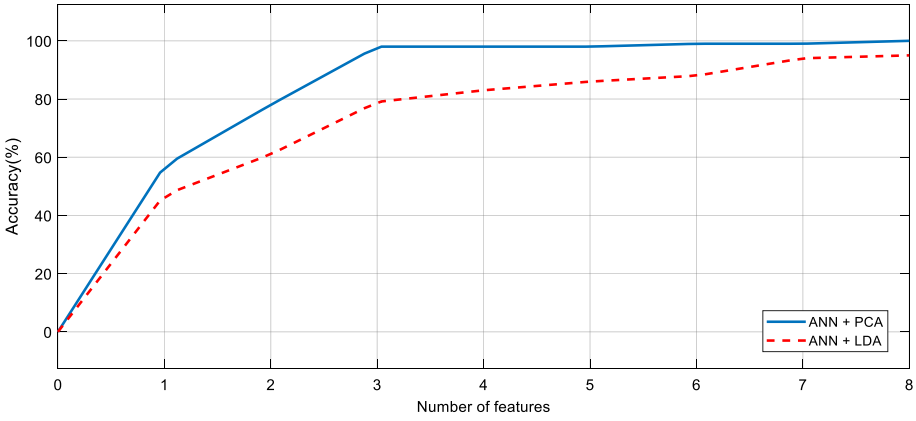

Fig. 24. ANN classification accuracy for different number of features using PCA and LDA.

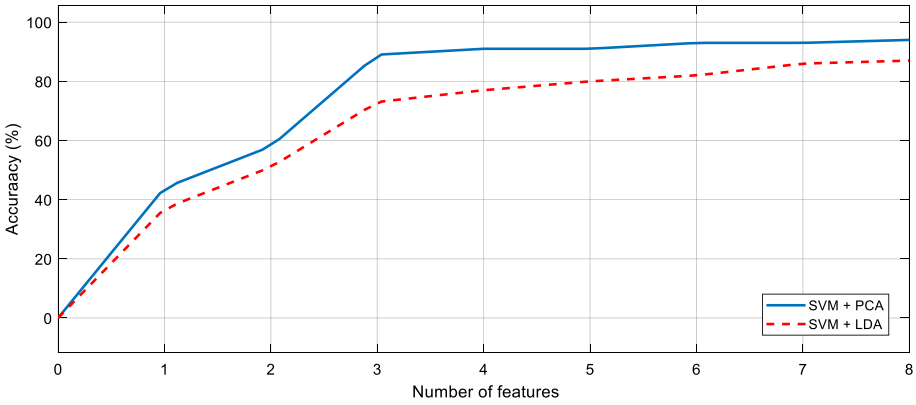

Fig. 25. SVM classification accuracy for different number of features using PCA and LDA.

Table 2
SVM and ANN classification accuracy using PCA and LDA.

Classification / Feature extraction	SVM	ANN
PCA (4 features)	89%	**98%**
LDA (3 features)	78%	89%

Table 3
Economic indicators of Mutriku wave power plant with and without classification-based diagnosis for predictive maintenance.

Indicator	Symbol	Unit	Value	
			without classification-based diagnosis	with classification-based diagnosis
Total operational OWCs	*TOWC*	–	14	14
Lifetime	n	year	20	20
Discount rate	r	%	15	15
Availability	a	%	91	**95**
Capacity factor	C_f	%	12.73	**13.28**
Annual Energy Production	AEP	MWh	288.833	**301.514**
Capital Expenditures	CapEx	€/kW	21621	21621
Operational Expenditures	OpEx	€/kW	1297	**1076**
Levelised Cost of Energy	LCoE	€/MWh	1174	**1112**

The purpose of calculating the economic indicators is to determine the values that would enable reaching a low LCoE in order to make OWC in particular and WECs in general competitive to other renewable energy technologies. Using the economic assumptions described in section 5.1. and the equations of the economic indicators defined in section 5.2., the parameters leading to the computations of the LCoE are summarized in Table 3.

Between January 2021 and December 2021 period the total amount of annual energy sold was 288833 *kW h* during an annual cumulative uptime of 7972 h and an annual cumulative downtime of 788 h, hence, using equation (24) the availability factor is 91% and using equation (25) the capacity factor is 12.73%.

With a reported total investment of 6.4M *EUR*, the CapEx is of *21321 €/kW* and an OpEx of around *1297.29 €/kW*. Hence, using equation (28) the LCoE is *1174 €/MWh*. This LCoE is considered high compared to other technologies and has to be reduced in order to meet the target LCoE by the year 2030 set by SET-Plan at *150 €/MWh* (Temporary Working Group Ocean Energy, 2018).

Using the developed classification-based OWC diagnosis to set a predictive maintenance instead of the unnecessary monthly and yearly preventive maintenances will:

- reduce maintenance costs by decreasing the OpEx until 17% (Ocean, 2013),
- reduce the downtime of the OWCs by 55% which will increase the availability to 95% (Pecher and Kofoed, 2017),
- increase uptime which increases the generated power by 4.4%, hence the capacity factor is increased to 13.28%.

Using equation (26) the improved AEP is 301514 *kW h* and using equation (28) the obtained LCoE with the predictive maintenance is *1112 €/MWh*.

From the results, it is obvious that the reduction of LCoE is highly dependent on the plant's availability, capacity factor and AEP. It is also important to note that the improvement of the availability and capacity factor is achieved through the implementation of a good predictive maintenance system. In addition, an adequate maintenance system will reduce the OpEx, which will further decrease the LCoE.

7. Conclusions

In the presented research work, a classification-based approach for diagnosing Power Take-Off systems in wave energy converters, with the aim of implementing a predictive maintenance strategy. The proposed concept utilizes experimental data from the plant to train classifier models that can predict the health status of each individual unit in the wave energy converters farm.

With over a decade of operation, the Mutriku wave power plant has been used as a study case to evaluate the suggested approach. The challenging environmental conditions in this case result in vibration in the Power Take-Off systems of the Oscillating Water Column units, leading to failures and breakages. These issues contribute to increased

downtime and a higher LCoE. The objective of this study is to diagnose and address the vibration problem in order to optimize the LCoE by employing an effective predictive maintenance strategy.

The presented work adopted two feature extraction methods namely the PCA and LDA to choose the most significant features for diagnosing OWCs. When using PCA it is found that it takes 4 features to achieve a cumulative explained variance of 96.74%. However, it takes 3 features to achieve a cumulative explained variance of 92.09% using LDA. Therefore, the first 3 common components were used namely the vibration, the rotational speed and the pressure to design and train the classification models.

Using the selected features, two classification methods were considered for this work the Support Vector Machine (SVM) and Artificial Neural Network (ANN) specifically the Muli-Layer Perceptron (MLP). The results showed that both methods successfully manage to perform with high accuracy. However, the ANN provided the best results with 98% accuracy against 81% from the SVM when using the PCA extraction method.

Based on the developed classification-based OWC diagnosis the economic indicators of the Mutriku wave power plant are calculated and showed that with the implementation of a predictive maintenance it's possible to reduce the OpEx until 17% and downtime to 55%, while increasing plant availability to reach 95% and eventually lead to a 5% reduction of the LCoE. This reduction has to be further improved in order to align with the objectives set by SET-Plan to reach a target LCoE of 150 €/MWh by the year 2030.

Finally, it could be remarked that, due to the scarce experimental real data on wave generation plants and the lack of similar studies on wave farms prognostics and cost reduction, this work could be extended and used as a reference for other wave farms, which could be relevant for investors and policymakers involved in the development of emerging wave-based renewable technologies.

Funding

This work was supported in part through project IT1555-22 funded by the Basque Government and through projects PID2021-123543OB-C21 and PID2021-123543OB-C22 funded by MCIN/AEI/10.13039/501100011033/FEDER, UE and through the Maria Zambrano grant MAZAM22/15 funded by UPV-EHU/MIU/Next Generation, EU.

CRediT authorship contribution statement

Fares M'zoughi: Conceptualization, Formal analysis, Investigation, Methodology, Validation, Visualization, Writing – original draft, Writing – review & editing. **Jon Lekube:** Conceptualization, Data curation, Formal analysis, Validation, Visualization, Writing – review & editing. **Aitor J. Garrido:** Conceptualization, Formal analysis, Funding acquisition, Methodology, Validation, Visualization, Writing – review & editing, Project administration. **Manuel De La Sen:** Conceptualization, Formal analysis, Validation, Visualization, Writing – review & editing. **Izaskun Garrido:** Conceptualization, Formal analysis, Funding acquisition, Methodology, Project administration, Validation, Visualization, Writing – review & editing.

Declaration of competing interest

The authors declare that they have no known competing financial interests or personal relationships that could have appeared to influence the work reported in this paper.

Data availability

Data will be made available on request.

Acknowledgements

The authors would like to thank the help and collaboration of the Basque Energy Agency (Ente Vasco de la Energía-EVE) and Biscay Marine Energy Platform-BiMEP for providing the real measured experimental data of the Mutriku wave power plant and the economic data.

The authors would also like to thank the Basque Government for funding their research work through project IT1555-22, the Ministry of Science and Innovation (MCIN) for funding their research work through projects PID2021-123543OB-C21 and PID2021-123543OB-C22 by (MCIN/AEI/10.13039/501100011033/FEDER, UE) and the University of the Basque Country (UPV/EHU) through the María Zambrano grant MAZAM22/15 funded by UPV-EHU/MIU/Next Generation, EU.

Nomenclature

Abbreviations

AEP	Annual Energy Production
ANN	Artificial Neural Network
AUC	Area Under Curve
BiMEP	Biscay Marine Energy Platform
CapEx	Capital Expenditure
IQR	Inter-Quartile Range
LCoE	Levelized Cost of Energy
LDA	Linear Discriminant analysis
LMA	Levenberg-Marquardt Algorithm
MLP	Multi-Layer Perceptron
MSE	Mean Squared Error
O&M	Operational and Maintenance
OLE	Object Linking and Embedding
OpEx	Operational Expenditure
OWC	Oscillating Water Column
PC	Principal Component
PCA	Principal Component Analysis
PLC	Programmable Logic Controller
PTO	Power Take- Off
PV	Present Value
ROC	Receiver Operating Characteristic
SVM	Support Vector Machine
TRL	Technology Readiness Level
WEC	Wave Energy Converter
WPP	Wave Power Plant

Symbols

a	availability factor
c	number of classes
C_f	capacity factor
C_i	set of data in the ith class
E_p	error penalty
$F(.)$	performance index
$\nabla F(.)$	gradient
$\nabla^2 F(.)$	Hessian matrix
g_i	cumulative energy
$J(.)$	Jacobian matrix
$K(.)$	kernel function
m_i	mean of the ith class
n	project lifetime
n_o	number of observations
n_v	number of variables
P_{Rated}	rated power
r	discount rate
S_B	between-class scatter matrix
S_W	matrix of within-class distribution
U	feature vector
$\boldsymbol{V}$	unitary matrix of eigenvectors
$\boldsymbol{v}_i$	eigenvectors

W	transformation matrix
w_{ji}	neural network weights
$\mathbf{X}$	matrix of data
Y_i	predicted output
Y_i	target output
Δw_{ji}	neural network weight's correction
Λ	diagonal matrix of eigenvalues
λ_i	eigenvalues
ξ_i	slack variables
Σ	covariance of the data matrix

References

Abdi, H., Williams, L.J., 2010. Principal component analysis. Wiley Interdisciplin. Rev.: Comput. Stat. 2 (4), 433–459.

Ahmad, A.S., Hassan, M.Y., Abdullah, M.P., Rahman, H.A., Hussin, F., Abdullah, H., Saidur, R., 2014. A review on applications of ANN and SVM for building electrical energy consumption forecasting. Renew. Sustain. Energy Rev. 33, 102–109.

Ampazis, N., Perantonis, S.J., 2000. Levenberg-Marquardt algorithm with adaptive momentum for the efficient training of feedforward networks. In: Proceedings of the IEEE-INNS-ENNS International Joint Conference on Neural Networks. IJCNN 2000. Neural Computing: New Challenges and Perspectives for *the* New Millennium, vol. 1, pp. 126–131.

Awad, M., Khanna, R., Awad, M., Khanna, R., 2015. Support vector machines for classification. In: Efficient Learning Machines: Theories, Concepts, and Applications for Engineers and System Designers. Apress, Berkeley, CA, pp. 39–66.

Boonyakitanont, P., Lek-Uthai, A., Chomtho, K., Songsiri, J., 2020. A review of feature extraction and performance evaluation in epileptic seizure detection using EEG. Biomed. Signal Process Control 57, 101702.

Bruck, M., Sandborn, P., Goudarzi, N., 2018. A levelized cost of energy (LCOE) model for wind farms that include power purchase agreements (PPAs). Renew. Energy 122, 131–139.

Cox, D.R., 2018. Analysis of Binary Data. Routledge.

Davis, R.A., Charlton, A.J., Godward, J., Jones, S.A., Harrison, M., Wilson, J.C., 2007. Adaptive binning: an improved binning method for metabolomics data using the undecimated wavelet transform. Chemometr. Intell. Lab. Syst. 85 (1), 144–154.

ETIP Ocean, 2019. Powering Homes Today, Powering Nations Tomorrow: Policy Solutions to Deliver Ocean Energy Industrial Roll-Out. Brussels.

European Commission, 2017. Tidal Turbine Power Take-Off Accelerator (TIPA). Available online: https://cordis.europa.eu/project/id/727793. (Accessed 28 October 2022).

European Commission, 2018. Innovative Method for Affordable Generation IN Ocean Energy (IMAGINE). Available online: https://cordis.europa.eu/project/id/764066. (Accessed 28 October 2022).

European Commission, 2019a. Next Evolution in Materials and Models for Ocean Energy (NEMMO). Available online: https://cordis.europa.eu/project/id/815278. (Accessed 28 October 2022).

European Commission, 2019b. PowerKite: Power Take-Off System for a Subsea Tidal Kite. Available online: https://cordis.europa.eu/project/id/654438. (Accessed 28 October 2022).

European Commission, 2019c. Open Sea Operating Experience to Reduce Wave Energy Cost (OPERA). Available online: https://cordis.europa.eu/project/id/654444. (Accessed 28 October 2022).

European Commission, 2020a. An EU Strategy to Harness the Potential of Offshore Renewable Energy for a Climate Neutral Future. Technical Report; European Commission: Brussels, Belgium. Available online: https://eur-lex.europa.eu/legal-content/EN/TXT/PDF/?uri=CELEX:52020DC0741&from=EN. (Accessed 28 October 2022).

European Commission, 2020b. WaveBoost: Advanced Braking Module with Cyclic Energy Recovery System (CERS) for Enhanced Reliability and Performance of Wave Energy Converters. Available online: https://cordis.europa.eu/project/id/727598. (Accessed 28 October 2022).

European Commission, SEA-TITAN, 2019. Surging Energy Absorption through Increasing Thrust and efficieNcy. Available online: https://cordis.europa.eu/project/id/764014. (Accessed 28 October 2022).

European Commission-SET Plan Secretariat, 2016. SET Plan–Declaration of Intent on Strategic Targets in the Context of an Initiative for Global Leadership in Ocean Energy. Technical Report; European Commission: Brussels, Belgium. Available online: https://setis.ec.europa.eu/system/files/2021-04/declaration_of_intent_ocean_0.pdf. (Accessed 28 October 2022).

Fisher, R.A., 1936. The use of multiple measurements in taxonomic problems. Annal. Eugenics 7 (2), 179–188.

Fs, M'zoughi, Bouallègue, S., Ayadi, M., Garrido, A.J., Garrido, I., 2017. Modelling and airflow control of an oscillating water column for wave power generation. In: 2017 4th International Conference on Control, Decision and Information Technologies (CoDIT), pp. 938–943.

Ghassabeh, Y.A., Rudzicz, F., Moghaddam, H.A., 2015. Fast incremental LDA feature extraction. Pattern Recogn. 48 (6), 1999–2012.

Ghosh, D., Singh, A., Shukla, K.K., Manchanda, K., 2019. Extended Karush-Kuhn-Tucker condition for constrained interval optimization problems and its application in support vector machines. Inf. Sci. 504, 276–292.

Hagan, M.T., Menhaj, M.B., 1994. Training feedforward networks with the Marquardt algorithm. IEEE Trans. Neural Network. 5 (6), 989–993.

Hasan, B.M., Abdulazeez, A.M., 2021. A review of principal component analysis algorithm for dimensionality reduction. J. Soft Comput. Data Min. 2 (1), 20–30.

Holyoak, K.J., 1987. Parallel distributed processing: explorations in the microstructure of cognition. Science 236, 992–997.

Ibarra-Berastegi, G., Sáenz, J., Ulazia, A., Serras, P., Esnaola, G., Garcia-Soto, C., 2018. Electricity production, capacity factor, and plant efficiency index at the Mutriku wave farm (2014–2016). Ocean Eng. 147, 20–29.

IEA-OES, 2018. Annual Report: an Overview of Ocean Energy Activities in 2018. IEA-OES, Lisbon. Available online: https://report2018.ocean-energy-systems.org/. (Accessed 28 October 2022).

IRENA, 2017. Renewable Power Generation Costs in 2017; Technical Report. International Renewable Energy Agency: Abu Dhabi, UAE. Available online: https://www.irena.org/publications/2018/jan/renewable-power-generation-costs-in-2017. (Accessed 10 November 2022).

Izenman, Alan Julian, 2013. Linear discriminant analysis. In: Modern Multivariate Statistical Techniques. Springer, New York, NY, pp. 237–280.

Izquierdo, S., Montanes, C., Dopazo, C., Fueyo, N., 2010. Analysis of CSP plants for the definition of energy policies: the influence on electricity cost of solar multiples, capacity factors and energy storage. Energy Pol. 38 (10), 6215–6221.

Jiang, Peng, 2011. Maintenance of wind turbine. Electr. Equip. 28 (6), 68–71.

Karyotakis, A., Bucknall, R., 2010. Planned intervention as a maintenance and repair strategy for offshore wind turbines. J. Marine Eng. Tech. 9 (1), 27–35.

Kiang, M.Y., 2003. A comparative assessment of classification methods. Decis. Support Syst. 35 (4), 441–454.

Kumar, V., Sachdeva, J., Gupta, I., Khandelwal, N., Ahuja, C.K., 2011. Classification of brain tumors using PCA-ANN. In: 2011 World Congress on Information and Communication Technologies, pp. 1079–1083.

Lee, S., 2021. Monte Carlo simulation using support vector machine and kernel density for failure probability estimation. Reliab. Eng. Syst. Saf. 209, 107481.

Lekube, J., Ajuria, O., Ibeas, M., Igareta, I., Gonzalez, A., 2018a. Fatigue and aerodynamic loss in wells turbines: Mutriku wave power plant case. In: Proceedings of the 7th International Conference on Ocean Energy (ICOE). Cherbourg, France, pp. 1–7.

Lekube, J., Garrido, A.J., Garrido, I., Otaola, E., Maseda, J., 2018b. Flow control in wells turbines for harnessing maximum wave power. Sensors 18 (2), 535.

Liu, J., Sun, J., Wang, S., 2006. Pattern recognition: an overview. IJCSNS Int. J. Computer Sci. Network Secur. 6 (6), 57–61.

Magagna, D., 2019. Ocean Energy Technology Development Report 2018. EUR 29907 EN, European Commission, Luxembourg. https://doi.org/10.2760/158132. JRC118296, 978-92-76-12428-3.

Magagna, D., 2020. Ocean energy - technology development report 2020, 978-92-76-27283-0. In: EUR 30509 EN, Publications Office of the European Union, Luxembourg. https://doi.org/10.2760/102596. JRC123159.

Magagna, D., Tacconi, P., 2019. About cost-reduction of ocean energy: lessons from Horizon 2020. SETIS 20, 11–12.

M'zoughi, F., Garrido, I., Garrido, A.J., De la Sen, M., 2020a. Fuzzy gain scheduled-sliding mode rotational speed control of an oscillating water column. IEEE Access 8, 45853–45873.

M'zoughi, F., Garrido, I., Garrido, A.J., De La Sen, M., 2020b. Rotational speed control using ANN-based MPPT for OWC based on surface elevation measurements. Appl. Sci. 10 (24), 8975.

M'zoughi, F., Garrido, I., Garrido, A.J., De La Sen, M., 2020c. ANN-based airflow control for an oscillating water column using surface elevation measurements. Sensors 20 (5), 1352.

Nova Innovation, "A World-First for Nova Innovation: the 'Holy Grail of Baseload Tidal Power," Nova Innov., Available online: https://www.novainnovation.com/news/news_/i/a-world-first-for-nova-innovation-the-holy-grail-of-baseload-tidal-power/ (accessed on 28 October 2022)..

Ocean, S.I., 2013. Ocean Energy: Cost of Energy and Cost Reduction Opportunities. Ocean Energy Sweden. Available online: https://oceanenergy-sweden.se/wp-content/uploads/2018/03/130501-si-ocean-cost-of-energy-report.pdf. (Accessed 10 November 2022).

OPERA Project, 2019. Final Assessment and Recommendations; Technical Report; Deliverable D7.5. Tecnalia for the OPERA Project. Available online: http://opera-h2020.eu/wp-content/uploads/2019/09/OPERA_D7.5-Final-assessment-andrecommendations_TECNALIA_20190724_v1.0.pdf. (Accessed 10 November 2022).

Paredes, M.G., Padilla-Rivera, A., Güereca, L.P., 2019. Life cycle assessment of ocean energy technologies: a systematic review. J. Mar. Sci. Eng. 7 (9), 322.

Pecher, A., Kofoed, J.P., 2017. Handbook of Ocean Wave Energy. Springer Nature.

Peng, Z., Chu, F., He, Y., 2002. Vibration signal analysis and feature extraction based on reassigned wavelet scalogram. J. Sound Vib. 253 (5), 1087–1100.

Pisner, D.A., Schnyer, D.M., 2020. Support vector machine. In: Machine Learning. Academic Press, pp. 101–121.

Quinlan, J.R., 2014. C4. 5: Programs for Machine Learning. Elsevier.

Ren, Z., Verma, A.S., Li, Y., Teuwen, J.J., Jiang, Z., 2021. Offshore wind turbine operations and maintenance: a state-of-the-art review. Renew. Sustain. Energy Rev. 144, 110886.

Sabella. Sabella D10 - France. Available online: https://www.sabella.bzh/en/projects/d10. (Accessed 28 October 2022).

Sierra-García, J.E., Santos, M., 2021. Redes neuronales y aprendizaje por refuerzo en el control de turbinas eólicas. Revista Iberoamericana de Automática e Informática industrial 18 (4), 327–335.

Sklansky, J., 1978. Image segmentation and feature extraction. IEEE Transactions on Systems, Man, and Cybernetics 8 (4), 237–247.

Suratgar, A.A., Tavakoli, M.B., Hoseinabadi, A., 2005. Modified Levenberg-Marquardt method for neural networks training. World Acad Sci Eng Technol 6 (1), 46–48.
Suthaharan, S., Suthaharan, S., 2016. Support vector machine. In: Machine Learning Models and Algorithms for Big Data Classification: Thinking with Examples for Effective Learning. Springer, Boston, MA, pp. 207–235.
Temporary Working Group Ocean Energy, 2018. SET-plan Ocean Energy—Implementation Plan. European Commission, Brussels, Belgium, pp. 1–50.
Têtu, A., Fernandez Chozas, J., 2020. Deliverable D8.1-Cost Database. Technical Report, LiftWEC–Development of a New Class of Wave Energy Converter Based on Hydrodynamic Lift Forces. Available online: https://liftwec.com/wp-content/uploads/2020/06/LW-D08-01-1x3-Cost-database.pdf. (Accessed 10 November 2022).
Têtu, A., Fernandez Chozas, J., 2021. A proposed guidance for the economic assessment of wave energy converters at early development stages. Energies 14 (15), 4699.
Thomas, É., É, Levrat, Iung, B., 2008. Overview on opportunistic maintenance. IFAC Proc. Vol. 41 (3), 245–250.
TiPA, "TIPA TURBINE SUCCESSFULLY COMPLETES SUBSEA TESTING," TiPA, Available online: https://www.tipa-h2020.eu/tipa-turbine-successfully-completes-subsea-testing/(accessed on 28 October 2022)..
Tomás-Rodríguez, M., Santos, M., 2019. Modelling and control of floating offshore wind turbines. Revista Iberoamericana de Automática e Informática Industrial 16 (4).
Torre-Enciso, Y., Ortubia, I., De Aguileta, L.L., Marqués, J., 2009. Mutriku wave power plant: from the thinking out to the reality. In: Proceedings of the 8th European Wave and Tidal Energy Conference, Uppsala, Sweden, vol. 710, pp. 319–329.
Umbra Cuscinette, S.p.A., 2017. Reciprocating Ball Screw Generator (ReBaS): WES Power Take off Stage 2 Project Public Report. WES, Inverness.
Verma, G.K., Tiwary, U.S., 2014. Multimodal fusion framework: a multiresolution approach for emotion classification and recognition from physiological signals. Neuroimage 102, 162–172.
Vidal, R., Ma, Y., Sastry, S.S., 2016. Principal component analysis. In: Generalized Principal Component Analysis. Springer, New York, USA, pp. 25–62.
Vinutha, H.P., Poornima, B., Sagar, B.M., 2018. Detection of outliers using interquartile range technique from intrusion dataset. In: Information and Decision Sciences: Proceedings of the 6th International Conference on FICTA. Springer Singapore, pp. 511–518.
Wave Energy Scotland. Emerge - electro-MEchanical reciprocating GEnerator. Available online: https://www.waveenergyscotland.co.uk/programmes/details/power-take-off/rebas-generator-reciprocating-ball-screw-generator/. (Accessed 28 October 2022).
Wen, J., Fang, X., Cui, J., Fei, L., Yan, K., Chen, Y., Xu, Y., 2018. Robust sparse linear discriminant analysis. IEEE Trans. Circ. Syst. Video Technol. 29 (2), 390–403.
Widodo, A., Yang, B.S., 2007. Support vector machine in machine condition monitoring and fault diagnosis. Mech. Syst. Signal Process. 21 (6), 2560–2574.
Wilamowski, B.M., Yu, H., 2010. Improved computation for levenberg–marquardt training. IEEE Trans. Neural Network. 21 (6), 930–937.
Wong, M.A., Lane, T., 1983. A *kth* nearest neighbour clustering procedure. J. Roy. Stat. Soc. B 45 (3), 362–368.
Yang, Z., Baraldi, P., Zio, E., 2022. A method for fault detection in multi-component systems based on sparse autoencoder-based deep neural networks. Reliab. Eng. Syst. Saf. 220, 108278.
Yeter, B., Garbatov, Y., Soares, C.G., 2020. Risk-based Maintenance Planning of Offshore Wind Turbine Farms, vol. 202. Reliability Engineering & System Safety, 107062.
Yu, H., Yang, J., 2001. A direct LDA algorithm for high-dimensional data—with application to face recognition. Pattern Recogn. 34 (10), 2067–2070.
Zhang, Z., Lyons, M., Schuster, M., Akamatsu, S., 1998. Comparison between geometry-based and gabor-wavelets-based facial expression recognition using multi-layer perceptron. In: Proceedings Third IEEE International Conference on Automatic Face and Gesture Recognition, pp. 454–459.
Zhu, W., Castanier, B., Bettayeb, B., 2019. A dynamic programming-based maintenance model of offshore wind turbine considering logistic delay and weather condition. Reliab. Eng. Syst. Saf. 190, 106512.